and G190A mainly reduce susceptibility to NVP [7–9]. Virologic failure with NNRTI-containing regimens generally associates with the emergence of NNRTI- and/or 3TC/FTC-resistant viruses [10,11]. In one study of drug-naïve persons comparing EFV with either Combivir (zidovudine/3TC) or Truvada (tenofovir and FTC), treatment failures at 96 weeks had viruses that were more commonly NNRTI-resistant or 3TC/FTC-resistant than tenofovir- resistant [12]. Likewise Margot et al. found K103N as the most common resistance mutation in patients failing regimens containing tenofovir, FTC and efavirenz or zidovudine, 3TC and EFV [13]. M184V and K103N/Y181C were seen in >10% of patients failing antiretroviral therapy in British Columbia, Canada during 1996 to 2003 [14]. Delaugerre et al. detected NNRTI-associated mutations in more than 98% of patients failing an efavirenz- or NVP-containing regimen [8].

Therefore, the availability of simple assays to measure NNRTI or 3TC/FTC resistance can be highly useful for managing first-line regimens. Rapid assays that can distinguish WT from 3TC/FTC- or NNRTI- resistant virus during virologic failure can inform decisions for switching regimens, which is particularly important in resource-limited settings with often single second-line regimens. Although sequencing is a widely used genotypic test to monitor drug resistance in resource-rich countries, the complexity and cost of this testing limits its utility for resource-limited countries with large HIV-infected populations. Thus, current treatment guidelines in resource-limited countries do not include resistance testing. We have previously described the use of a sensitive biochemical assay (Amp-RT) to measure the enzymatic activity of reverse transcriptase (RT) of HIV-1 in plasma and assess its susceptibility to antiretroviral drugs [15]. Like other RT assays that are broadly reactive on all retroviruses, Amp-RT can detect generically RT activity from diverse retrovirus groups including HIV-1 non-subtype B and HIV-2 [15,16]. We have previously demonstrated that this technology can also be used for HIV drug-resistance testing and have shown that biochemical detection of NNRTI and 3TC resistance by this method correlates well with genotypic and replication-based phenotypic assays [9,17]. Here, we describe the development of improved Amp-RT assays that use real-time PCR detection and simplified virus capture from plasma. The real-time PCR readout replaces the previously used ELISA-based detection of PCR products and provides a rapid and cost-effective quantitation. Likewise we demonstrate the utility of virus capture from plasma by magnetic beads that eliminate the need for ultracentrifugation. We evaluated Amp-RT-based assays that screen for resistance to 3TC and NVP in a large collection of clinical specimens with known drug-resistance profiles, and show data that support the promise of this testing strategy for drug-resistance management.

Materials and Methods

Ethics Statement

Specimens were anonymous residual diagnostic material from subjects who provided written consent for HIV testing. The CDC Institutional Review Board determined that this testing did not involve identifiable human subjects and has approved the study.

Assay Optimization

The optimization of assay conditions was done by unblinded testing of 140 plasma samples. They consisted of 114 subtype B and 26 non-B subtypes (two A, 22 recombinant AG, two unknown). In addition, the specificity was evaluated by testing 160 samples from HIV- seronegative blood donors and 14 HIV-seropositive specimens that had undetectable RNA viral loads (<40 copies/ml). Assay validation was done by blinded testing 253 (229 subtype B, 14 subtype C, 6 subtype A, 1 subtype D, and 3 recombinant including CRF nomenclatures AG and AE) plasma samples collected at the BC Centre for Excellence in HIV/AIDS (BC, Canada). The median RNA virus load in these samples was 4.28+/−0.84 $\log_{10}$ copies/ml and ranged between 2.29 and 5.88.

Viral load Measurement and Sequencing

Roche Amplicor Version 1.5, with a limit of detection of 50 copies/ml was used for quantitating HIV RNA in plasma. Standard population-based sequencing was performed with a limit of detection of approximately 20–30% for a minority sequence variant as described in [18]. The region sequenced typically covered codon 1 to 400 of the RT.

Reference Viruses and Drugs

The following isolates were used as control reference viruses in each experiment: HXB2, xxBRU$_{pitt}$, and HIV-1$_{SUM\ 9}$ as WT viruses; M184V$_{pitt}$ as 3TC-resistant virus carrying the M184V mutation [13]. X403-4 and X82-5 are NVP-resistant isolates carrying the Y181C or K103N/Y181C mutations, respectively [9]. Nevirapine was obtained from the NIH AIDS Research & Reference Program (Rockville, MD). 3TC-triphosphate was synthesized by Sierra Bioresearch (Tucson, AZ). Both drugs were aliquoted and kept at −80°C.

Principle of the Amp-RT Assay

Amp-RT is an ultrasensitive RT assay that uses PCR to detect RT-generated DNA of an exogenous non-retroviral heteropolymeric RNA template from the encephalomyocarditis virus (EMCV) genome [15]. Levels of EMCV DNA generated by HIV-1 RT in a plasma specimen are quantified by real-time PCR as described below.

RT Activity Detection by Amp-RT

To detect RT activity in plasma specimens, 250 µl of plasma was first clarified at 10,000 g for 5 min and then ultracentrifuged at 99,000 g for 1 h at 4°C. Virus pellets were concentrated in a final volume of 100 µl of 1× RTCDR buffer (50 mM Tris HCl, 50 mM KCl, 10 mM $MgCl_2$, 0.5 mM EGTA, 2 mM DTT, 0.06% NP-40). A known amount of HXB2 particles (1×10^5) spiked in an HIV-1 seronegative plasma was included in each experiment to control for the quality of the ultracentrifugation procedure. The mean and standard deviation were determined in 35 runs. The range for the control was defined as mean ±3× standard deviation. Thus an individual ultracentrifugation run was considered valid when the control with 1×10^5 HXB2 particles yielded a Ct value between 18.37 and 28.97.

To eliminate the need for ultracentrifugation, an alternative method was evaluated for virus capture from plasma by using magnetic beads coated with CD44 monoclonal antibody (µMultiMACS^{TM} VitalVirus HIV Isolation Kit; Miltenyi Biotec, Auburn, CA). CD44 is one of the host cell proteins present on HIV 1 particles [19]. CD44 been shown to be suitable for capture of HIV-1 particless from patient samples [20] and can be used for virus genotyping even from patients with no detectable viral load [21]. After clarifying the plasma at 10,000 g for 5 min, 200 µl were incubated with 20 µl microbeads for 10 min at room temperature. Then, the mixture was applied to MACS separation columns and washed 4 times. HIV-1 particles bound to the column were dissolved in 100 µl 1×RTCDR, yielding HIV RT in

enzymatically active form. The eluate was immediately used in the RT reaction or stored at −70 °C.

Levels of RT activity were measured in duplicate using 96-well plates. Briefly, 4 µl of virus pellets or eluants were added to 16 µl of RT buffer containing 50 mM Tris HCl, 50 mM KCl, 10 mM $MgCl_2$, 0.5 mM EGTA, 2 mM DTT, 10 µM dCTP, 120 µM dATP, dGTP, and dTTP, 1 µM antisense primer 262R (5′-CAACGTCTTCAAGCGTCGAAT-3′), 0.20 ng × μl^{-1} EMCV RNA, 0.10 u × μl^{-1} RNasin, and 0.06% NP-40. As a competitive inhibitor, 3TC-TP inhibits RT activity more efficiently when dCTP concentration is reduced resulting in less 3TC-TP in the assay. We have previously shown by titrations of dCTP and 3TC-TP that 10 µM of dCTP was optimal for detecting both RT activity and its inhibition by 3TC-TP [17]. The RT reaction was carried out for 2 h at 37°C, followed by a 5 min inactivation of HIV-1 RT at 95°C. To evaluate the susceptibility of the RT for 3TC and NVP, parallel RT reactions were done in the presence of 50 µM 3TC-triphosphate (3TC-TP) and 50 µM NVP.

cDNA Quantification by Real-Time PCR

Levels of RT-generated EMCV cDNA were quantified by real-time PCR in the TaqMan™ format. Briefly, 10 µl of RT-generated EMCV cDNA were added to 40 µl of PCR buffer containing 1× AmpliTaq Gold buffer, 4.0 mM MgCl2, 250 µM dNTP, 0.5 µM sense primer EMCF1 (5′-CTCCCAT-CAGGTTGTGCAGCGACC-3′), 0.5 µM antisense primer 262R, 0.192 µM FAM-labeled probe 158T (5′-AAGGTGAGAG-CAAGCCTCGCAAAGACA-3′), and 0.05 U × μl^{-1} AmpliTaq Gold polymerase. The PCR reaction mixtures were then subjected to 45 cycles at 95°C for 15 s and 60°C for 1 min. Oligonucleotides EMCF1 and 262R, as well as the probe 158T were obtained from Scientific Resources Program, CDC.

Measuring Enzymatic RT Resistance to Lamivudine and Nevirapine

Susceptibility of HIV-1 RT for 3TC-TP or NVP was measured by comparing the level of inhibition of the Amp-RT signal in reactions done in the presence of drug relative to reactions without drug. Samples were categorized as sensitive or resistant based on the differences in Ct values (ΔCt) seen in reactions done in the presence and absence of drug. One screening concentration was established for 3TC and NVP based on the results from the 140 samples tested unblinded. The screening concentration was selected to best differentiate in "sensitive" and "resistant" corresponding to the respective genotype. We considered only samples that had an average Ct_0 value below 36.25 cycles to prevent misinterpretation of resistant samples because of signal instability close to the detection limit. Samples with enzymatic susceptibility data that did not correlate with resistance mutations were tested further to determine Amp-RT IC50 and IC90 values. To this end we applied inhibitor concentrations ranging from 5 to 500 µM, depending on the ΔCt obtained with 50 µM inhibitor concentration. IC50 values were determined by linear regression.

Statistics

Statistical evaluation and graphic representation of the data was done with with GraphPad Prism 4 (GraphPad Software Inc., USA). We derived ΔCt cut-off values for differentiating between sensitive and resistant from the 140 samples tested unblinded for validation. For 3TC and NVP we defined the cut off value as the mean ΔCt of all genotypically resistant specimens using the screening concentrations for 3TC and NVP plus 3× the standard deviation.

Results

Correlation between RT Levels by Amp-RT and RNA Virus Loads

We first tested 140 clinical isolates with known RT genotypes. The median log_{10} RNA virus loads of the 114 subtype B samples was 4.2±0.8 log_{10} (range 2.4–5.5) and correlated well with the Ct values determined by Amp-RT (r = 0.68, 95% confidence interval, 0.77–0.57, $P<0.0001$). A similar correlation between the median log_{10} RNA virus loads and Ct values measured Amp-RT was seen in the 26 non-B subtypes samples (r = 0.69, 95% CI interval, 0.85–0.41, $P<0.0001$), illustrating that Ct values measured by Amp-RT represent a good indication of plasma virus loads. (data not shown). The specificity of the assay was evaluated by testing 160 samples from HIV-seronegative blood donors. The results showed a mean Ct_0 value of 44.6±1.1 (range 40.2, >45). A similar mean Ct_0 value (43.8±1.9, range 39.6−45) was seen in 15 HIV-seropositive specimens that had undetectable RNA virus loads (<50 Geq × ml^{-1}). Sixty control reactions done in the absence of RT enzyme yielded no signal within 45 PCR cycles. Thus, no RNA-negative sample yielded lower Ct values than the threshold for clinical samples to be included in the resistance evaluation (36.25).

Detection of 3TC and Nevirapine Resistance

We next evaluated the ability of the assay to discriminate between 3TC- and NVP-sensitive and resistant viruses. Figure 1 shows the differences of Ct values (ΔCt) for 3TC and NVP seen in all the isolates tested unblinded. The mean ΔCt for 3TC in 56 WT isolates was 6.2±2.5 (range 0.29–11.2) and was significantly higher ($P<0.0001$) than the mean ΔCt seen in the 55 3TC-resistant isolates that had the M184V mutation (0.2±0.8, range -1.6–2.1, Figure 1A). Figure 1B shows that the mean ΔCt for NVP seen in 83 WT isolates was 7.42±3.18 (range 0.235–15.9) compared to a mean ΔCt value of 0.484±0.963 (range -1.85–2.15) seen in 28 NVP-resistant samples carrying K103N, Y181C/I, Y188L, or G190A/Q ($P<0.0001$). These findings confirm that a single drug concentration of 50 µM 3TC or NVP can reliably differentiate between WT and resistant isolates as a screening assay.

We next selected the respective ΔCt cut-off values based on the mean ΔCt+3.0 SD observed in all the mutant isolates, resulting at 2.66 and 3.28 for 3TC and NVP. Using these ΔCt cut-off values, we found a very high concordance between Amp-RT phenotype and RT genotype. For instance, all 55 samples that had M184V were classified as 3TC-resistant while all 28 samples carrying NVP-associated mutations were considered NVP-resistant. On the other hand, 52 of the 56 samples with 184 M (92.9%) were interpreted 3TC-sensitive, while 79 of the 83 samples lacking detectable NVP-associated mutations (95.2%) were classified as NVP-sensitive. Of the 8 discordant samples (4 for 3TC and 4 for NVP), five had ΔCt values close to the assay cut-offs (data not shown).

Assay Variability

We evaluated inter-assay variability of ΔCt values by comparing the values observed in our control WT, 3TC- and NVP-resistant isolates tested in 14 independent experiments. The ΔCt values for HXB2 WT ranged from 7.9 to 10.8 with a mean of 9.5 for 3TC, and from 7.9 to 11.9 for NVP (mean 9.73). The 3TC-resistant control strain $M184V_{pitt}$ yielded a mean ΔCt of 0.9 (range 0.3–1.6) for 3TC and 8.8 for NVP (range 6.9–11.0). On the other hand the NVP-resistant strain Y188C X403-4 resulted in a mean of 8.4 (range 6.9–9.7) for 3TC and 1.9 (range 1.3–2.7) for NVP. The variability was much lower than the ΔCt cut-off values for the

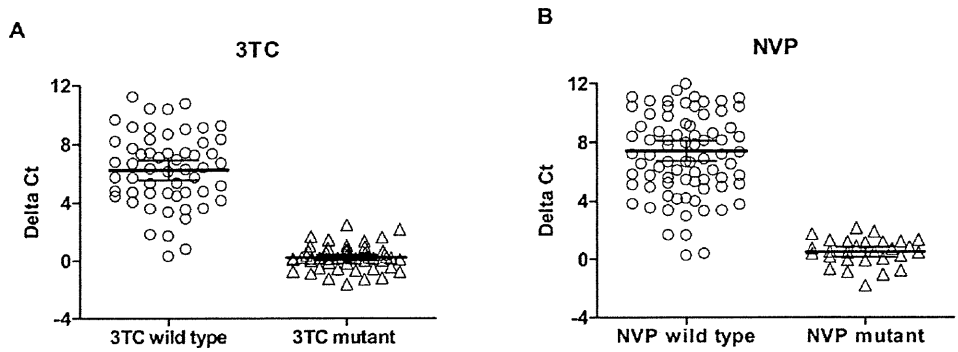

Figure 1. RT inhibition in 140 clinical isolates after virus concentration by ultracentrifugation. Genotypes had been classified into wild type and mutant. Scatter plots show delta Ct values (threshold cycle difference between inhibited and uninhibited reaction) measured with 50 μM 3TC (A) and NVP (B). Horizontal bars indicate the respective mean values and the 95% confidence intervals. For mutants delta22Ct values are close to 0 for both drugs illustrating that mutant RT enzymes are virtually not inhibited by 50 μM drug concentrations.
doi:10.1371/journal.pone.0022019.g001

screening assays. Thus no sample will be erroneously classified sensitive because of assay variation.

Assay Performance on Clinical Samples

We analyzed 173 specimens blinded, with genotypes revealed only after the testing. Applying our previously defined cut-off values, 99 samples were classified as 3TC-sensitive and 74 as 3TC-resistant (Table 1) by Amp-RT. Of the 99 samples 3TC-sensitive by Amp-RT, 94 (96%) were genotypically WT, 3 had a mixture of M184 M/V, and 2 showed M184 V. The two samples with M184 V had ΔCt values of 2.7 and 2.8, which were close to the assay cut-off (2.66). Of the 8 samples that had an M184 M/V mixture, 5 were Amp-RT resistant and 3 had ΔCt values below 4.1. Of the 74 samples with phenotypic resistance to 3TC, 70 (94%) had the M184 V or M184I mutations. Among these samples, there were 64 184 V, 1 had 184I, and 5 had 184 V/M mixtures. In four samples, phenotypic resistance to 3TC was seen in the absence of detectable 184 V or 184I. We tested two of them (ΔCt values 0.8 and 1.2) with higher 3TC concentrations (150, 500, and 1000 μM). The results further confirmed reduced 3TC susceptibility in these two isolates (data not shown). However, the levels of 3TC resistance were lower than those seen in an isolate carrying the 184 V mutation. In three of the four strains with reduced enzymatic susceptibility to 3TC in the absence of 184I/V we found the mutation V118I which has been previously associated with low-level enzymatic resistance to 3TC-TP [22].

Of the 173 samples tested for NVP resistance, 82 were classified as sensitive and 91 as resistant. Enzymatic NVP resistance was associated with the presence of K103N, Y181C/I, Y188L, G190A/Q, or K238N in 88 of the 91 samples. The other 3 samples showed NVP resistance in the absence of any of these 5 mutations. Seventy-three of the 82 samples classified as NVP sensitive had WT genotypes. Of the other remaining 9 samples, 2 had the K103N mutation and a ΔCt value close to the assay cut-off (3.8 and 3.4), and 7 had mixtures of WT and mutant genotypes. Overall, the current findings demonstrate the ability of the new Amp-RT format to detect phenotypic resistance to 3TC or NVP.

Assay Performance on Bead-Captured HIV-1

We also tested 162 blinded samples with a simplified protocol replacing ultracentrifugation by concentrating the virus with CD44-coated magnetic beads (μMultiMACS™ VitalVirus HIV Isolation Kit). The summarized results are illustrated in scatter plots in Figure 2. Our cut-off values categorized the samples as shown in Table 2. Of 110 samples categorized sensitive for 3TC by Amp-RT only one had the mutation M184V, the corresponding ΔC of 2.79 was only slightly above the cut-off (Figure 2A). Conversely, 52 were enzymatically resistant to 3TC with 51 strains harboring M184V. For NVP 102 specimens were Amp-RT sensitive (Figure 2B). No NVP resistance mutation had been found in 95, one had a mixed genotype K103 K/N and 6 contained the mutations K103N, G190A, or Y188L. Four of the six samples were further analyzed with different NVP concentrations to allow for IC50 determination. Fold changes in IC50 values relative to WT HIV-1_{HXB2} were 9.8, 6.4, 3.4, and 1.0 indicating enzymatic NVP resistance for three 3 of 4 specimens. Fifty-nine specimens were found to be enzymatically NVP-resistant. Of these, 56 had NNRTI mutations and 3 had no NNRTI-resistance mutations. In summary, there was a good correlation between genotype and enzymatic resistance in both formats of virus preparation.

Discussion

Current treatment guidelines in the developed world recommend the use of drug-resistance testing for the management of patients receiving antiretroviral therapy. However, because such testing relies mainly on sequencing or recombinant virus phenotyping, which are costly and complex, it has remained largely unavailable for the vast majority of patient populations receiving ART in resource-limited settings. Thus, simpler and less expensive drug resistance technologies may improve patient management. Previously explored technology relied on detecting and phenotyping HIV-associated RT activity in plasma by ultrasensitive biochemical assays [9,17,23,24]. In this study we describe an improved biochemical approach to resistance testing for NNRTI and 3TC/FTC. The principle is based on our previously reported Amp-RT assays [9,17] but has been improved in two major ways. First, we include real-time PCR for the detection of Amp-RT product which eliminates the need of ELISA quantitation of the PCR products, thus reducing time and cost. Secondly, we describe a method of HIV capture from plasma by magnetic beads, eliminating the need for ultracentrifugation and reducing cost and complexity.

Conventionally, phenotypic resistance is reported as fold changes in IC50 values over a reference WT virus. Since this approach requires testing of multiple drug concentrations we sought to evaluate a screening method with only one drug

Table 1. Blinded drug-resistance testing with the 50 μM screening format after virus enrichment by ultracentrifugation.

	3TC			NVP		
Genotype	**Wild type**	**Mixed genotype**	**Mutant[a]**	**Wild type**	**Mixed genotype**	**Mutant[b]**
Amp-RT sensitive	94	3	2	73	7	2
Amp-RT resistant	4	5	65	3	11	77
Total	98	8	67	76	18	79

[a]including the mutations M184V/I.
[b]including the mutations K103N, Y181C/I, Y188L, G190A/Q, or K238N.
doi:10.1371/journal.pone.0022019.t001

concentration to help simplify testing. We have found previously that this approach was feasible, given the high level of resistance conferred by M184V and many NNRTI mutations. By testing large numbers of mutant and WT clinical specimens we show here that inhibition with the 50 μM screening concentration correlated well with the absence of genotypic markers of resistance to 3TC/FTC. This screening concentration is close to the 3TC-TP concentration that inhibits WT enzymatic activity by 100% (IC100). We demonstrate that enzymatic 3TC resistance was strongly associated with M184I/V. In addition, we also found that the mutation V118I was associated with enzymatic 3TC resistance in the absence of M184V in 3 of 4 cases. In vitro, V118 is reported to confer resistance to 3TC and other nucleoside analogues only in combination with other mutations like D67N and T215Y [22]. However, consistent with our results, Girouard and colleagues detected a 21.7-fold enzymatic resistance to 3TC-TP in RTs harboring just V118I [25]. The clinical significance of this resistance is unclear and requires more study. NNRTI mutations are common in ART-treated populations. Our data also show that the screening Amp-RT format detecting resistance to NVP correlated with the presence of K103N, Y181C/I, Y188L, and G190A/Q. Thus, all primary mutations conferring resistance to NNRTIs are detected. While K103N or Y188L confer high cross-resistance between NVP and EFV[7], Y181C/I/V is associated with only moderate resistance to EVF. Thus, the use of NVP in the assay allowed the detection of resistance mutations that may be selected by either NVP or EFV. However, further work may be needed to determine if EFV is more suitable than NVP for detecting resistance by particular NNRTI mutations that confer higher resistance to EFV than NVP and whether the use of EFV would have detected resistance in few mutant samples that showed WT results in the current assay.

Despite the strong correlation between genotype and enzymatic resistance, few specimens showed discrepant results. The reasons for the discrepancies are not clear but could be related to a number of factors including a wrong genotype because of sequencing error, imperfect cut-offs values, mutations currently not known to cause enzymatic resistance, or mixed genotypes that are inconsistently detected genotypically or enzymatically. While enzymatic IC50 determination clarified the discrepancies in many samples, further phenotypic testing by culture-based methods and additional genotypic analysis by ultradeep sequencing for minority or mixed resistance, and inclusion of mutations in the connection domain in RT that confer NNRI resistance could help resolve the source of the residual discrepant results [26].

Although this work has focused on assays for 3TC/FTC and NNRTI resistance because of the high prevalence in virologic failure and the high level of resistance, this testing approach can be adapted to other RT inhibitors, including new-generation NNRTIs and other nucleoside analogs. Such assays will require careful development that takes into account the level of enzymatic resistance found in the mutants, and the need for a screening or IC50-based testing format. One important improvement in our testing is the capture of virus by magnetic beads, which eliminated the need for ultracentrifugation and the associated cost, labor, and maintenance. We demonstrate the utility of virus capture with magnetic beads containing antibodies against CD44, a host-cell protein that is commonly incorporated on the surface of HIV-1 particles. This method has the advantages of allowing high throughput and automated processing. Overall, in contrast to

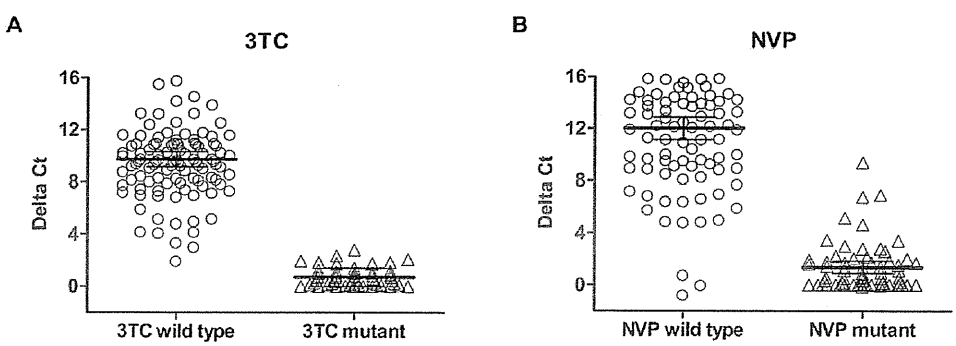

Figure 2. RT inhibition in 162 samples after virus concentration with CD44-coated beads. Genotypes had been classified into wild type and mutant. Scatter plots show delta Ct values (threshold cycle difference between inhibited and uninhibited reaction) measured with 50 μM 3TC (A) and NVP (B). Horizontal bars indicate the respective mean values and the 95% confidence intervals. The established cut-offs for both drugs classified the isolates as summarized in Table 2. Data correlate well to those obtained by ultracentrifugation (Figure 1) with slightly more discrepancies between geno- and phenotype for NVP.
doi:10.1371/journal.pone.0022019.g002

Table 2. Blinded drug-resistance testing with the 50 μM screening format after virus enrichment by CD44-coated beads.

	3TC			NVP		
Genotype	Wild type	Mixed genotype	Mutant[a]	Wild type	Mixed genotype	Mutant[b]
Amp-RT sensitive	109	0	1	95	1	6
Amp-RT resistant	1	0	51	3	0	56
Total	110	0	52	98	1	62

[a]including the mutations M184V/I.
[b]including the mutations K103N, Y181C/I, Y188L, G190A/Q, or K238N.
doi:10.1371/journal.pone.0022019.t002

conventional sequencing or cell-culture based phenotypic assays, the enzymatic Amp-RT testing described in this work does not require special and expensive instrumentation or equipment but instead a real-time PCR cycler and common equipment available in clinical virology laboratories with biosafety level 2 capacity. Additional studies geared to evaluating the assay in a resource-limited setting would include further simplified storage conditions, sensitivity to repeated freezing and thawing of the reagents and interference with other infectious agents present in the samples. The described assays have a short turnaround time and have the advantage of being subtype-independent. The reaction carried out in the absence of drug can also be used as a marker of virus load as demonstrated in the good correlation with RNA loads in this and previous studies [23]. In conclusion, we demonstrate the strong potential for a simplified drug-resistance testing strategy based on sensitive enzymatic assays for two key drug-resistance profiles that are of particular importance for first-line regimens. Our data strongly support expanded clinical evaluation and standardization of this testing approach.

Acknowledgments

We are grateful to John Nkengasong (CDC, Atlanta) for providing the non-B HIV sample set and to Sal Butera for advice in the use of magnetic beads. Lamivudine and nevirapine were obtained through the AIDS Research and Reference Reagent Program, Division of AIDS, NIAID.

The findings and conclusions in this paper are those of the authors and do not necessarily represent the views of the Centers for Disease Control and Prevention.

Author Contributions

Conceived and designed the experiments: DH ADG PRH WH. Performed the experiments: DH ADG. Analyzed the data: DH ADG. Contributed reagents/materials/analysis tools: PRH ICDJ TN JGGL. Wrote the paper: DH WH.

References

1. Richman DD (2001) HIV chemotherapy. Nature 410: 995–1001.
2. Deeks SG (2003) Treatment of antiretroviral-drug-resistant HIV-1 infection. Lancet 362: 2002–11.
3. Johnson VA, Brun-Vezinet F, Clotet B, Gunthard HF, Kuritzkes DR, et al. (2009) Update of the drug resistance mutations in HIV-1: December 2009. Top HIV Med 17: 138–45.
4. EuroGuidelines Group for HIV Resistance (2001) Clinical and laboratory guidelines for the use of HIV-1 drug resistance testing as part of treatment management: recommendations for the European setting. The EuroGUidelines Group for HIV resistance. Aids 15: 309–20.
5. Margot NA, Waters JM, Miller MD (2006) In vitro human immunodeficiency virus type 1 resistance selections with combinations of tenofovir and emtricitabine or abacavir and lamivudine. Antimicrob Agents Chemother 50: 4087–95.
6. Wainberg MA, Hsu M, Gu Z, Borkow G, Parniak MA (1996) Effectiveness of 3TC in HIV clinical trials may be due in part to the M184V substitution in 3TC-resistant HIV-1 reverse transcriptase. Aids 10(Suppl 5): 3–10.
7. Bacheler L, Jeffrey S, Hanna G, D'Aquila R, Wallace L, et al. (2001) Genotypic correlates of phenotypic resistance to efavirenz in virus isolates from patients failing nonnucleoside reverse transcriptase inhibitor therapy. J Virol 75: 4999–5008.
8. Delaugerre C, Rohban R, Simon A, Mouroux M, Tricot C, et al. (2001) Resistance profile and cross-resistance of HIV-1 among patients failing a non-nucleoside reverse transcriptase inhibitor-containing regimen. J Med Virol 65: 445–8.
9. Vazquez-Rosales G, García-Lerma JG, Yamamoto S, Switzer WM, Havlir D, et al. (1999) Rapid screening of phenotypic resistance to nevirapine by direct analysis of HIV type 1 reverse transcriptase activity in plasma. AIDS Res Hum Retroviruses 15: 1191–200.
10. Barth RE, van der Loeff MFS, Schuurman R, Hoepelmon AIM, Wensing AMJ (2010) Virological follow-up of adult patients in antiretroviral treatment programmes in sub-Saharan Africa: a systematic review. Lancet Infectious Diseases 10: 155–166.
11. Wallis CL, Mellors JW, Venter WDF, Sanne I, Stevens W (2010) Varied Patterns of HIV-1 Drug Resistance on Failing First-Line Antiretroviral Therapy in South Africa. Jaids-Journal of Acquired Immune Deficiency Syndromes 53: 480–484.
12. Pozniak AL, Gallant JE, DeJesus E, Arribas JR, Gazzard B, et al. (2006) Tenofovir disoproxil fumarate, emtricitabine, and efavirenz versus fixed-dose zidovudine/lamivudine and efavirenz in antiretroviral-naive patients: virologic, immunologic, and morphologic changes–a 96-week analysis. J Acquir Immune Defic Syndr 43: 535–40.
13. Margot NA, Enejosa J, Cheng AK, Miller MD, McColl DJ (2009) Development of HIV-1 Drug Resistance Through 144 Weeks in Antiretroviral-Naive Subjects on Emtricitabine, Tenofovir Disoproxil Fumarate, and Efavirenz Compared With Lamivudine/Zidovudine and Efavirenz in Study GS-01-934. J Acquir Immune Defic Syndr.
14. Cheung PK, Wynhoven B, Harrigan PR (2004) 2004: which HIV-1 drug resistance mutations are common in clinical practice? AIDS Rev 6: 107–16.
15. Heneine W, Yamamoto S, Switzer WM, Spira TJ, Folks TM (1995) Detection of reverse transcriptase by a highly sensitive assay in sera from persons infected with human immunodeficiency virus type 1. J Infect Dis 171: 1210–6.
16. García-Lerma JG, Soriano V, Mas A, Quinones-Mateu ME, Arts EJ, et al. (2000) Quantitation of human immunodeficiency virus type 1 group O load in plasma by measuring reverse transcriptase activity. Journal of Clinical Microbiology 38: 402–405.
17. García-Lerma J, Schinazi RF, Juodawlkis AS, Soriano V, Lin Y, et al. (1999) A rapid non-culture-based assay for clinical monitoring of phenotypic resistance of human immunodeficiency virus type 1 to lamivudine (3TC). Antimicrob Agents Chemother 43: 264–70.
18. Galli RA, Sattha B, Wynhoven B, O'Shaughnessy MV, Harrigan PR (2003) Sources and magnitude of intralaboratory variability in a sequence-based genotypic assay for human immunodeficiency virus type 1 drug resistance. Journal of Clinical Microbiology 41: 2900–2907.
19. Tremblay MJ, Fortin JF, Cantin R (1998) The acquisition of host-encoded proteins by nascent HIV-I. Immunology Today 19: 346–351.
20. Piantadosi A, Humes D, Chohan B, McClelland RS, Overbaugh J (2009) Analysis of the percentage of human immunodeficiency virus type 1 sequences that are hypermutated and markers of disease progression in a longitudinal cohort, including one individual with a partially defective Vif. J Virol 83: 7805–7814.
21. Lopez CA, Vazquez M, Hill MD, Colon MC, Porrata-Doria T, et al. (2010) Characterization of HIV-1 RNA forms in the plasma of patients undergoing successful HAART. Arch Virol 155: 895–903.
22. Romano L, Venturi G, Bloor S, Harrigan R, Larder BA, et al. (2002) Broad nucleoside-analogue resistance implications for human immunodeficiency virus type 1 reverse-transcriptase mutations at codons 44 and 118. J Infect Dis 185: 898–904.
23. Garcia-Lerma JG, Yamamoto S, Gomez-Cano M, Soriano V, Green TA, et al. (1998) Measurement of human immunodeficiency virus type 1 plasma virus load

based on reverse transcriptase (RT) activity: evidence of variabilities in levels of virion-associated RT. J Infect Dis 177: 1221–9.
24. Napravnik S, Cachafeiro A, Stewart P, Eron JJ, Jr., Fiscus SA (2009) HIV-1 viral load and phenotypic antiretroviral drug resistance assays based on reverse transcriptase activity in comparison to amplification based HIV-1 RNA and genotypic assays. J Clin Virol 47: 18–22.
25. Girouard M, Diallo K, Marchand B, McCormick S, Gotte M (2003) Mutations E44D and V118I in the reverse transcriptase of HIV-1 play distinct mechanistic roles in dual resistance to AZT and 3TC. J Biol Chem 278: 34403–10.
26. Yap SH, Sheen CW, Fahey J, Zanin M, Tyssen D, et al. (2007) N348I in the connection domain of HIV-1 reverse transcriptase confers zidovudine and nevirapine resistance. Plos Medicine 4: 1887–1900.

Int. J. Radiation Oncology Biol. Phys., Vol. 80, No. 2, pp. 540–548, 2011

0360-3016/$ - see front matter

ELSEVIER

doi:10.1016/j.ijrobp.2010.12.065

BIOLOGY CONTRIBUTION

TARGETING THE AKT/GSK3β/CYCLIN D1/CDK4 SURVIVAL SIGNALING PATHWAY FOR ERADICATION OF TUMOR RADIORESISTANCE ACQUIRED BY FRACTIONATED RADIOTHERAPY

TSUTOMU SHIMURA, PH.D.,* SATOSHI KAKUDA, M. MED.,* YASUSHI OCHIAI, B.SC.,* YOSHIKAZU KUWAHARA, PH.D.,* YOSHIHIRO TAKAI, M.D., PH.D.,† AND MANABU FUKUMOTO, M.D., PH.D.*

*Department of Pathology, Institute of Development, Aging and Cancer, Tohoku University, Sendai, Japan; †Department of Radiology and Radiation Oncology, Hirosaki University School of Medicine, Hirosaki, Japan

Purpose: Radioresistance is a major cause of treatment failure of radiotherapy (RT) in human cancer. We have recently revealed that acquired radioresistance of tumor cells induced by fractionated radiation is attributable to cyclin D1 overexpression as a consequence of the downregulation of GSK3β-dependent cyclin D1 proteolysis mediated by a constitutively activated serine-threonine kinase, AKT. This prompted us to hypothesize that targeting the AKT/GSK3β/cyclin D1 pathway may improve fractionated RT by suppressing acquired radioresistance of tumor cells.

Methods and Materials: Two human tumor cell lines with acquired radioresistance were exposed to X-rays after incubation with either an AKT inhibitor, AKT/PKB signaling inhibitor-2 (API-2), or a Cdk4 inhibitor (Cdk4-I). Cells were then subjected to immunoblotting, clonogenic survival assay, cell growth analysis, and cell death analysis with TUNEL and annexin V staining. *In vivo* radiosensitivity was assessed by growth of human tumors xenografted into nude mice.

Results: Treatment with API-2 resulted in downregulation of cyclin D1 expression in cells with acquired radioresistance. Cellular radioresistance disappeared completely both *in vitro* and *in vivo* with accompanying apoptosis when treated with API-2. Furthermore, inhibition of cyclin D1/Cdk4 by Cdk4-I was sufficient for abolishing radioresistance. Treatment with either API-2 or Cdk4-I was also effective in suppressing resistance to cis-platinum (II)-diamine-dichloride in the cells with acquired radioresistance. Interestingly, the radiosensitizing effect of API-2 was canceled by overexpression of cyclin D1 whereas Cdk4-I was still able to sensitize cells with cyclin D1 overexpression.

Conclusion: Cyclin D1/Cdk4 is a critical target of the AKT survival signaling pathway responsible for tumor radioresistance. Targeting the AKT/GSK3β/cyclin D1/Cdk4 pathway would provide a novel approach to improve fractionated RT and would have an impact on tumor eradication in combination with chemotherapy. © 2011 Elsevier Inc.

Radioresistance, Fractionated radiation, AKT inhibitor, AKT, Cyclin D1.

INTRODUCTION

Radiotherapy (RT) is one of the major modalities of cancer treatment with rather better functional preservation and less systemic influences. RT can be given in combination with surgery or chemotherapy. General protocol of fractionated RT consists of daily exposures to a fraction dose of around 2 Gy for 5–7 weeks. Although tumors receive a large total dose by multiple fractionated radiation (FR), they sometimes recur with radioresistance (1). The fundamental mechanisms behind the resistance of tumor cells to RT remain largely elusive. We have recently revealed that human tumor cells receiving FR at a moderate dose of X-rays every 12 h for 1 month acquire radioresistance through the activation of AKT/glycogen synthase kinase-3β (GSK3β)/cyclin D1 pathway. This pathway is constitutively activated by a positive feedback loop mediated through the cyclin D1 overexpression cycle triggered by FR (2).

Accumulating evidence suggests that the phosphatidylinositol-3-OH kinase (PI3K)/AKT signaling pathway is a major contributor to radioresistance (3–7). However, critical targets of AKT in tumor radioresistance

Reprint requests to: Manabu Fukumoto, M.D. Ph.D., Department of Pathology, Institute of Development, Aging and Cancer, Tohoku University, 4-1 Seiryo-machi, Sendai 980-8575, Japan. Tel. +81-022-717-8507; Fax: +81-022-717-8512. E-mail: fukumoto@idac.tohoku.ac.jp

The first two authors made equal contributions to the research.

Supported by the Grant-in-Aid for young scientists (Wakate-B-21710054); the Grant-in-Aid from Ministry of Education, Culture, Sports, Science and Technology; grants from the Ministry of Health, Labour and Welfare of Japan; and by the "Frontier Science Research Program" in the Center for Interdisciplinary Research, Tohoku University.

Conflict of interest: none.

Acknowledgment—We thank Dr Ohtsura Niwa for critical reading of the paper. We thank Dr. J. Alan Diehl for providing pFleX-cyclin D1 expression vectors.

Received Sept 7, 2010, and in revised form Dec 18, 2010. Accepted for publication Dec 20, 2010.

remain to be elucidated. The PI3K/AKT signaling pathway regulates cellular processes of proliferation and survival (8, 9). DNA-PK mediates AKT phosphorylation at serine 473 to promote cell survival against lethal damage induced by genotoxic stress (10, 11). AKT regulates cell proliferation by stabilization of cyclin D1 through GSK3β inactivation. Cyclin D1 mediates cell cycle progression through G1- to S-phase by binding to Cdk4. Activated AKT phosphorylates serine 9 of GSK3β to inactivate its kinase activity on threonine 286 of cyclin D1, which then blocks the nuclear export and the cytoplasmic proteasomal degradation of cyclin D1 (12).

In the present study, we experimentally examined whether the failure of fractionated RT is a consequence of acquired radioresistance of tumor cells. Using 31FR-31NR HeLa cells with acquired radioresistance, we analyzed the susceptibility of cells to 2 Gy FR *in vitro* and 3 Gy FR *in vivo*. We further assessed whether the radioresistance of the cells against FR can be suppressed targeting the AKT/GSK3β/cyclin D1/Cdk4 pathway either with AKT inhibitor, API-2 or a Cdk-4 inhibitor (Cdk4-I), 2-bromo-12,13-dihydro-5H-indolo[2,3-a]pyrrolo[3,4-c]carbazole-5,7(6H)-dione (13). We found that cyclin D1/Cdk4 is a major target of the AKT signaling pathway to suppress tumor radioresistance acquired by fractionated RT.

METHODS AND MATERIALS

Cell culture condition and drugs

HeLa, a cervical cancer cell line, and HepG2, a human liver cancer cell line, were obtained from the Cell Resource Center for Biomedical Research, IDAC, Tohoku University. Cells were grown in a RPMI1640 medium (Sigma, St. Louis, MO) supplemented with a 5% heat-inactivated fetal calf serum. An AKT inhibitor of API-2 (14) and a Cdk4 inhibitor of Cdk4-I (13) were purchased from Calbiochem (San Diego, CA). Cells were incubated with API-2 or Cdk4-I for 24 h before treatment either with ionizing radiation or cis-platinum (II)-diamine-dichloride (CDDP) (Nippon Kayaku, Tokyo, Japan).

Irradiation experiments

Both *in vivo* and *in vitro* irradiations were performed using a 150-KVp X-ray generator (Model MBR-1520R, Hitachi, Tokyo, Japan) with a 0.5 mm Cu and 0.1 mm Al filter at a dose rate of 1.0 Gy/min. FR consisting of 2 Gy per fraction were delivered in the cells 6 days per week *in vitro*.

Clonogenic assay

Cells were seeded in 60 mm dish coated with 0.1% gelatin (Wako Pure Chemical Industries, Ltd., Osaka, Japan) at 1×10^3 or 5×10^3 cells per dish. After irradiation, cells were incubated for 10 days until colonies were visible. They were fixed with ethanol for 30 min and stained with Giemsa solution (Merck & Co. Inc., Blue Bell, PA). The colonies of more than 50 cells were counted under a light microscope.

Cell growth assay

Cells (5×10^5) were seeded in a 25 cm^2 flask (Thermo Fisher Scientific/Nunc, Waltham, MA), incubated overnight and irradiated daily with 2 Gy of FR for the indicated number of days. Growth rates were monitored by counting cell number twice a week. When the total cell number was $>5 \times 10^5$, cells were subcultured to 5×10^5 cells in a flask.

Western blot analyses

Western blotting was performed as described previously (15). Proteins were separated by sodium-lauryl-sulfate-polyacrylamide gel electrophoresis and transferred electrophoretically to PVDF membranes (Bio-Rad, Richmond, CA). Membranes were blocked with 5% (W/v) phospho-blocker (Cell Biolabs Inc., San Diego, CA) for 1 h and incubated with anti-β-actin (A2066, Sigma), anti-AKT (4685, Cell Signaling, Beverly, MA), anti-phospho-AKT-Ser473 (4060, Cell Signaling) and anti-cleaved caspase-3 (9664, Cell Signaling) for 1 h at room temperature or overnight at 4°C. Membranes were then incubated for 1 h at room temperature with the secondary antibody of HRP-conjugated goat anti-rabbit immunoglobulin G (Nichirei Bioscience, Tokyo, Japan). The protein bands were visualized with Chemi-Lumi One L Western blotting substrate (Nacalai Tesque, Kyoto, Japan).

TUNEL assay

TUNEL assay was performed using an In Situ Cell Death Detection Kit (Roche, Lewes, UK). Cells grown on 18 mm × 18 mm cover slips were washed with phosphate-buffered saline (PBS) and fixed with 4% paraformaldehyde in PBS for 1 h. They were rinsed with PBS and permeabilized with 0.1% tironX-100 for 2 min on ice. The coverslips were incubated with TUNEL reaction mixture for 1 h at 37°C. They were then washed three times with PBS and counterstained with Hochest 33258 (Wako Pure Chemical Industries). Images were captured by an epifluorescence microscopy (Nikon Corporation, Tokyo, Japan) using a 40 × objective lens. We counted >100 cells at each point.

Annexin V staining

Apoptotic cells were identified and quantified using an annexin V-FITC apoptosis detection kit (Bio Vision, Mountain View, CA) following the manufacturer's protocol. Cells were stained with annexin V-FITC and propidium iodide (PI) 48 h after treatment with radiation or CDDP. Annexin V-positive apoptotic cells were analyzed by the FACScan (Cytomics FC500, Becton Dickinson, Mountain View, CA).

Animal experiments

The study design was approved by the Ethical Committee of Tohoku University. Male BALB/c nu/nu mice of 5 weeks of age were used in the present experiment. All mice were maintained in our animal facility on a 12 light and 12 dark h cycle under a controlled temperature (23 ± 2°C). For the transplantation, 5×10^6 cells of HeLa 0FR and HeLa 31FR-31NR in 100 μL of saline were injected into the right and the left legs of the mice, respectively. Mice were treated with API-2 (1 mg/kg/day) in 0.1 mL of 20% DMSO (vehicle) (Nacalai Tesque, Kyoto, Japan) or vehicle only for control every 24 h for 7 days when the tumor size reached about 40 mm^3. For the treatment of radiation plus API-2 or DMSO, the first drug treatment was performed 24 h before the start of FR. The other parts of the body were protected by a lead shield. The size of tumors was measured with calipers. The tumor volume (V) was estimated by $V = \text{length} \times \text{width}^2/2$.

Statistical analysis

Error bars represent standard deviations; in some cases the standard deviations were too small to be visible on the histogram. All the experiments were repeated at least three times with independent samples. Student's *t*-test was used for the analysis. A single asterisk and double asterisks indicate the significance ($p < 0.01$) and ($p < 0.05$), respectively.

RESULTS

Radioresistance to FR by acquired radioresistance of human tumor cells

To establish human tumor cell lines with acquired radioresistance, HeLa and HepG2 were exposed to 0.5 Gy of X-rays every 12 h for more than a month and further cultured without irradiation for more than 31 days. Those were designated as 31FR-31NR cells (2). To evaluate resistance to FR, we compared colony survival of 31FR-31NR cells with control 0FR cells after FR at 2 Gy/fraction/day, which is commonly used in standard fractionated RT (Fig. 1A). Survival rates decreased in response to the increased dose in 0FR cells of HeLa and HepG2. In contrast, the survival rate of 31FR-31NR HeLa cells decreased up to 42 Gy of X-rays but stayed constant thereafter, indicating that 31FR-31NR HeLa cells were radioresistant to 2 Gy of FR. Compared with 0FR HepG2 cells, significant radioresistance was only seen at 14 Gy in 31FR-31NR HepG2 cells; however, the phenotype disappeared thereafter.

We next investigated cell growth of 0FR and 31FR-31NR cells of HeLa and HepG2 undergoing 2 Gy of FR (Fig. 1B). The growth of 0FR HeLa cells reached a plateau following 18-day FR, indicating that the cells were not able to divide under FR exposure any further. In contrast, 31FR-31NR HeLa cells continued to grow during FR exposure for 32 days (Fig. 1B, left panel). Although 31FR-31NR HepG2 cells grew faster than 0FR HepG2 cells during FR exposure, radioresistance to FR was not seen in 31FR-31NR HepG2 cells at 2 Gy/fraction/day (Fig. 1B, right panel). These cells showed radioresistance to 1.5 Gy/fraction/day compared with 0 FR HepG2 cells (Supplemental Fig. 1). These results and the colony data in Fig. 1A demonstrated that 31FR-31NR HeLa cells, but not 31FR-31NR HepG2 cells, exhibited radioresistance to 2 Gy of FR.

We thought that resistance of 31FR-31NR HeLa cells against 2 Gy of FR is attributable to the constitutive activation of the AKT/GSK3β/cyclin D1/Cdk4 pathway. To suppress the pathway, we used an AKT inhibitor, API-2 or a Cdk4 inhibitor, Cdk4-I. Growth suppression by 2 Gy of FR was more rapid by the combination of FR with API-2 than FR alone in all the cell lines examined (Fig. 1B). Interestingly, radioresistance of 31FR-31NR HeLa cells against FR was completely suppressed by API-2 treatment (Fig. 1B, left panel). As we reported previously, 1.9 μM of Cdk4-I could suppress cyclin D1/Cdk4-dependent phosphorylation of Rb at Serine 795 in 0FR and 31FR-31NR cells of HeLa (2). Cdk4-I alone could not block cell growth in all the cell lines examined (Supplemental Fig. 2). As expected, combination of Cdk4-I and FR could suppress radioresistance of 31FR-31NR HeLa cells (Fig. 1C). Therefore, we assumed that the AKT/GSK3β/cyclin D1/Cdk4 pathway is essential for acquired radioresistance to FR and is a potential target for the reversal of radioresistance.

To further determine the importance of cyclin D1 on radioresistance to FR, we examined whether or not the radiosensitization effect of API-2 was diminished by cyclin D1 overexpression. As reported, cells acquire radioresistance by overexpression of non-degradable cyclin D1 mutant (cyclin D1-T286A) (2). API-2 had no effects on radiosensitivity of HeLa and HepG2 cells with cyclin D1-T286A. This result demonstrated that cyclin D1 overexpression is sufficient to confer radioresistance of tumor cells to FR in the absence of AKT activation. In contrast, inactivation of cyclin D1/Cdk4 with Cdk4-I suppressed radioresistance induced by cyclin D1-T286A transfection (Fig. 1D). Thus, cyclin D1/Cdk4 is essential and is a major target of the AKT pathway responsible for radioresistance of tumor cells.

Transient growth suppression by AKT inactivation with API-2

To elucidate the effect of API-2, we examined AKT phosphorylation at Serine 473 of 0FR and of 31FR-31NR HeLa cells in the presence of API-2 and after removal of API-2. 31FR-31NR HeLa cells harbored high level of AKT activation compared with 0FR HeLa cells. Treatment with API-2 for 24 h attenuated phosphorylated-AKT (P-AKT) in 0FR and 31FR-31NR HeLa cells (Fig. 2A). The signal of P-AKT became gradually intensified with time after the removal of API-2 from 0FR and 31FR-31NR HeLa cells (Fig. 2A). Cell growth retarded during API-2 treatment for 24, 72, and 120 h in 0FR and 31FR-31NR cells (Fig. 2B, Supplemental Fig. 3). After removal of API-2, cell growth resumed in parallel with recovery of P-AKT signal (Fig. 2A, B). These results demonstrated that API-2 mediated growth suppression was reversible.

Induction of apoptosis after irradiation in cells with acquired radioresistance by inactivation of the AKT pathway

To evaluate the effect of API-2 on cell survival, apoptosis and mitotic catastrophe were investigated 48 h after treatment with radiation alone, API-2 alone, or radiation plus API-2 by nuclear staining with Hoechst33258 in 0FR and 31FR-31NR HeLa cells (Fig. 3A). Cells with the round and condensed nucleus (Fig. 3A, arrowheads), and multinucleated cells (Fig. 3A, arrows) represent apoptosis and mitotic catastrophe, respectively. Cells undergoing mitotic catastrophe increased in accordance with the increase of the dose in all the cell lines examined. However, the frequency of radiation-induced mitotic catastrophe was significantly lower in 31FR-31NR HeLa cells compared to 0FR HeLa cells (Fig. 3A, left lower panel). High level of AKT activation in 31FR-31NR HeLa cells was thought to be associated with less induction of cell death after irradiation. Therefore, we thought that inhibition of the AKT pathway with API-2 may increase radiation-induced cell death in

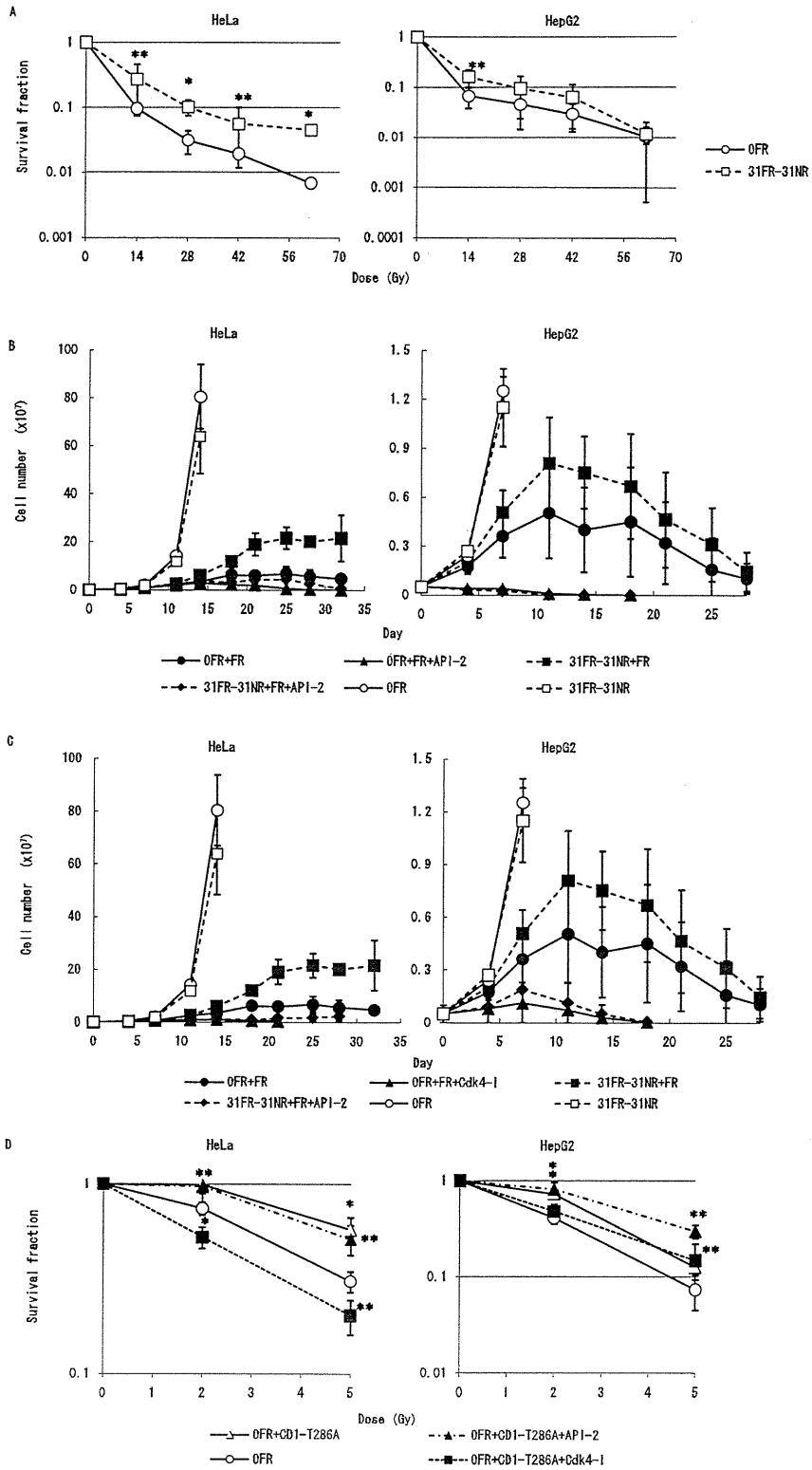

Fig. 1. Suppression of radioresistance by an AKT inhibitor, API-2, or a Cdk4 inhibitor, Cdk4-I (A). Survival curves of 0 fractionated radiation (FR) (open circle) and 31FR-31NR cells (open square) of HeLa on the left and those of HepG2 on the right, after irradiation. (B) Cell growth in 0FR cells with 2 Gy of FR (closed circle), 0FR cells with FR plus API-2 (closed triangle), nonirradiated 0FR cells (open circle), 31FR-31NR cells with FR (closed square), 31FR-31NR cells with FR plus API-2 (closed diamond), and nonirradiated 31FR-31NR cells (open square). Cells were treated with 20 μM of API-2 for 24 h/wk. (C) Growth suppression by treatment with a Cdk4 inhibitor, Cdk4-I. Cells were treated with 1.9 μM of the Cdk4-I for 24 h/wk. (D) Survival curves of 0FR cells, 0FR cells with FLAG-tagged cyclin D1-T286A, and 0FR cells with FLAG-tagged cyclin D1-T286A treated either with API-2 or Cdk4-I are shown.

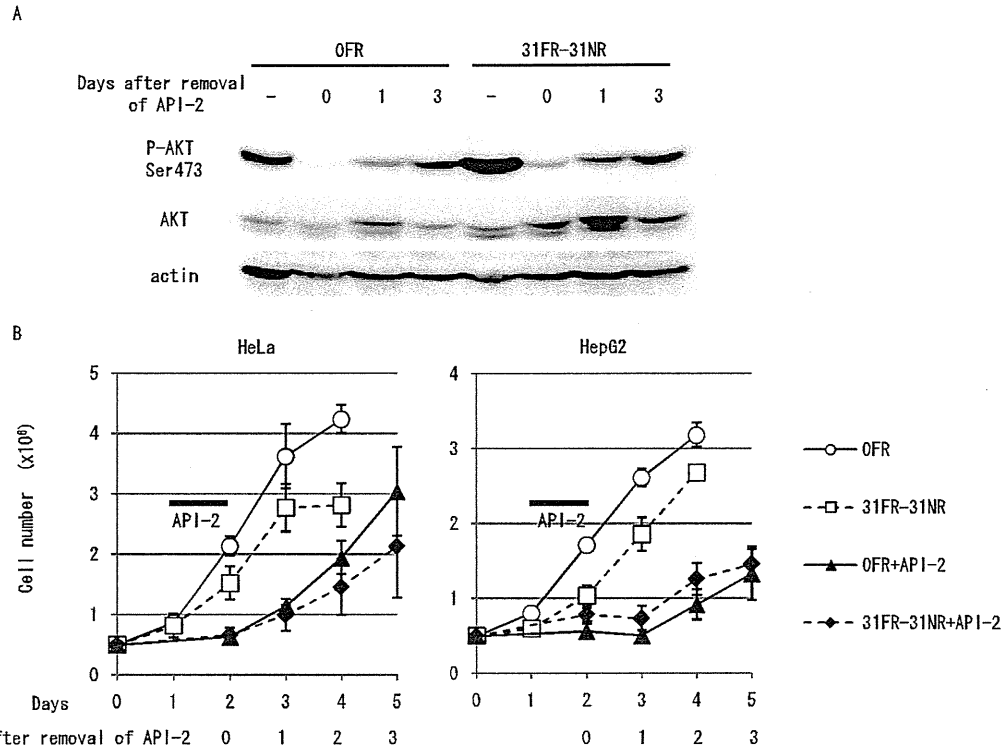

Fig. 2. Transient growth suppression by API-2 in 0 fractionated radiation (FR) and 31FR-31NR HeLa cells (A) Western blotting of phosphorylated-AKT-serine 473 (P-AKT Ser473), AKT, and β-actin in 0FR and 31FR-31NR cells. (B) Growth retardation by API-2 in 0FR and 31FR-31NR cells. Cells were treated with 20 μM of API-2 for 24 h from day 1 to day 2 as indicated by black lines.

radioresistant 31FR-31NR HeLa cells. API-2 alone had no effects on induction of mitotic catastrophe and apoptosis in both 0FR and 31FR-31NR HeLa cells (Fig. 3A). The incidence of mitotic catastrophe induced by irradiation was not different between cells treated with/without API-2 in both 0FR and 31FR-31NR HeLa cells. In contrast, radiation-induced apoptosis was significantly increased by API-2-mediated inactivation of the AKT pathway in 0FR and 31FR-31NR HeLa cells.

Apoptosis in 31FR-31NR HeLa cells was also determined by the TUNEL assay which detects DNA double-strand breaks (Fig. 3B) or annexin V-staining (Fig. 3C). TUNEL-positive cells were hardly detected by radiation alone, but they appeared after treatment with radiation plus API-2 in both 0FR and 31FR-31NR HeLa cells (Fig. 3B). Increased apoptosis was also seen by annexin V staining in 0FR and 31FR-31NR HeLa cells treated with radiation plus API-2 compared with radiation alone (Fig. 3C). Similarly, Cdk4 inhibitor increased the incidence of radiation-induced apoptosis in 0FR and 31FR-31NR HeLa cells (Fig. 3C).

Activation of molecular pathways of apoptosis was further investigated in 31FR-31NR HeLa cells by detection of active/cleaved caspase-3. A faint signal of the processing of caspase-3 to an active form was detected 48 h after 5 Gy irradiation in 0FR and 31FR-31NR HeLa cells. This active caspase-3 signal was intensified by pretreatment with API-2 before irradiation with decreased P-AKT signals. These results demonstrated that inhibition of the AKT/GSK3β/cyclin D1 pathway led to caspase-3 activation and induction of apoptosis after irradiation in 31FR-31NR HeLa cells accompanied with loss of radioresistance.

The role of API-2 for suppression of CDDP-resistance in 31FR-31NR cells

Cyclin D1 overexpression is implicated in drug resistance to CDDP of tumor cells (16). Because cyclin D1 was overexpressed in 31FR-31NR cells, we speculated that 31FR-31NR cells are resistant to CDDP, and examined their sensitivity to CDDP by colony assay (Fig. 4A). As expected, 31FR-31NR cells were more resistant to CDDP at doses up to 0.5 μM compared with 0FR cells (Fig. 4A). Thus, 31FR-31NR cells acquired resistance to both CDDP and radiation. As well as suppression of radioresistance, both API-2 and Cdk4-I had a role in suppressing CDDP resistance in 31FR-31NR cells of HeLa and HepG2 (Fig. 4A, 4B). The frequency of apoptosis was significantly higher in 31FR-31NR HeLa cells by treatment with CDDP plus API-2 than with CDDP alone (Fig. 4C). These results indicated that the AKT pathway is important not only for radioresistance but also for CDDP-resistance in cells with acquired radioresistance.

Targeting the AKT pathway for suppression of in vivo *radioresistance in 31FR-31NR HeLa tumors*

To determine the importance of the AKT pathway in tumor radioresistance, 0FR and 31FR-31NR HeLa cells were transplanted into right and left legs of nude mice

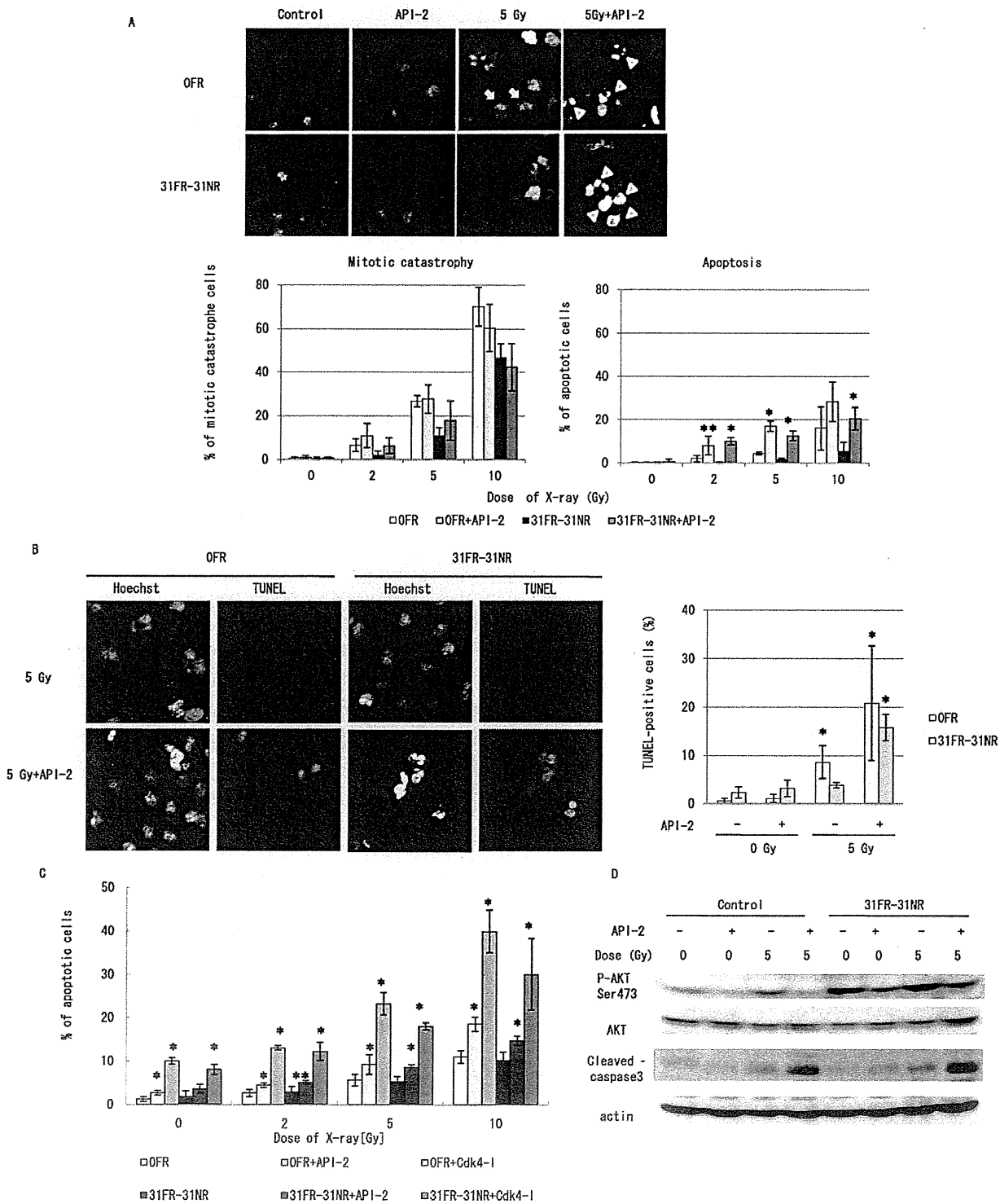

Fig. 3. Induction of apoptosis after irradiation by inactivation of the AKT pathway. (A) Nuclear staining with Heochst33258 in 0 fractionated radiation (FR) and 31FR-31NR HeLa cells treated with API-2 alone, radiation, and radiation plus API-2. Incidence of mitotic catastrophe and apoptosis was shown on the lower panels. We counted more than 100 cells at each point. Asterisks indicate significant increase of apoptosis in 0FR and 31FR-31NR cells by API-2 treatment in comparison to those cells without API-2. (B) TUNEL assay in 0FR and 31FR-31NR cells after radiation with and without API-2. Percentages of TUNEL-positive cells were shown on the right panel. (C) Annexin V staining in 0FR and 31FR-31NR cells. Asterisks indicate significant increase of Annexin V–positive cells by API-2 or Cdk4-I treatment in 0FR and 31FR-31NR cells in comparison to those without drugs. (D) Western blotting of p-AKT Ser473, AKT, cleaved-caspase-3 (the active form), and β-actin in 0 FR and 31FR-31NR cells treated with radiation, API-2 alone, and combination of radiation and API-2.

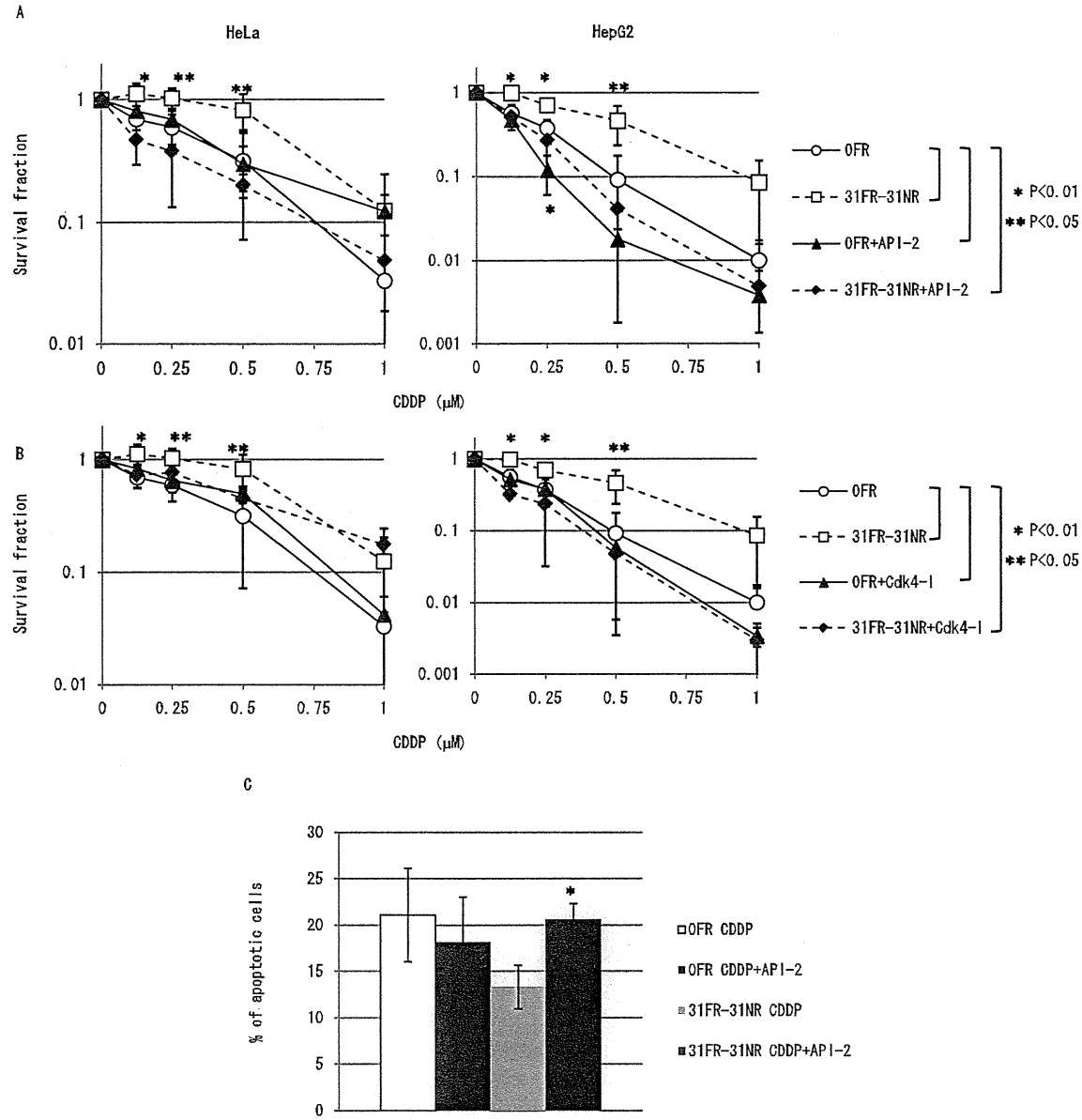

Fig. 4. Suppression of CDDP-resistance in 31FR-31NR cells by inactivation of the AKT pathway (A) Survival curves of 0 fractionated radiation (FR) cells (open circle), 0FR cells with API-2 (closed triangle), 31FR-31NR cells (open square), and 31FR-31NR cells with API-2 (closed diamond) of HeLa on the left and those of HepG2 on the right, after treatment with CDDP for 12 h. (B) Survival curves of 0FR cells (open circle), 0FR cells with Cdk4-I (closed triangle), 31FR-31NR cells (open square), and 31FR-31NR cells with Cdk4-I (closed diamond) of HeLa on the left and those of HepG2 on the right, after treatment with CDDP for 12 h. (C) Annexin V staining of 0FR cells with CDDP, 0FR cells with CDDP plus API-2, 31FR-31NR cells with CDDP, and 31FR-31NR cells with CDDP plus API-2. Cells were treated with 0.5 μM of CDDP for 12 h, incubated for further 48 hours without CDDP and stained with annexin V.

respectively and had their radiosensitivity examined *in vivo*. When the tumors reached a size about 40 mm^3, the mice were divided into four groups: DMSO (control group), API-2 (API-2 group), FR with DMSO (FR group), and FR with API-2 (FR+API-2 group). The schedule of FR was composed of 3 Gy/day for 7 days. Tumor growth was monitored by daily measurement of tumor size (Fig. 5A). Growth of 0FR tumors was not significantly different between control and API-2 groups. However, the growth of 31FR-31NR tumors of API-2 group was retarded compared with control tumors (Fig. 5A, left panel). The growth of 0FR tumors was inhibited by FR both in FR and FR+API-2 groups (Fig. 5A, right panel). The volume of 31FR-31NR tumors of FR group increased, indicating that 31FR-31NR cells were also radioresistant *in vivo*. However, these *in vivo* radioresistance of 31FR-31NR tumors was successfully suppressed by the combination of FR and API-2 (Fig. 5A, right panel). Histological findings revealed that viability and density of tumor cells without FR were not significantly different among all the groups. We examined the area of tumor tissues with the most viable cells. Compared with nonirradiated tumors, apoptotic cells with pyknotic nuclei were frequently

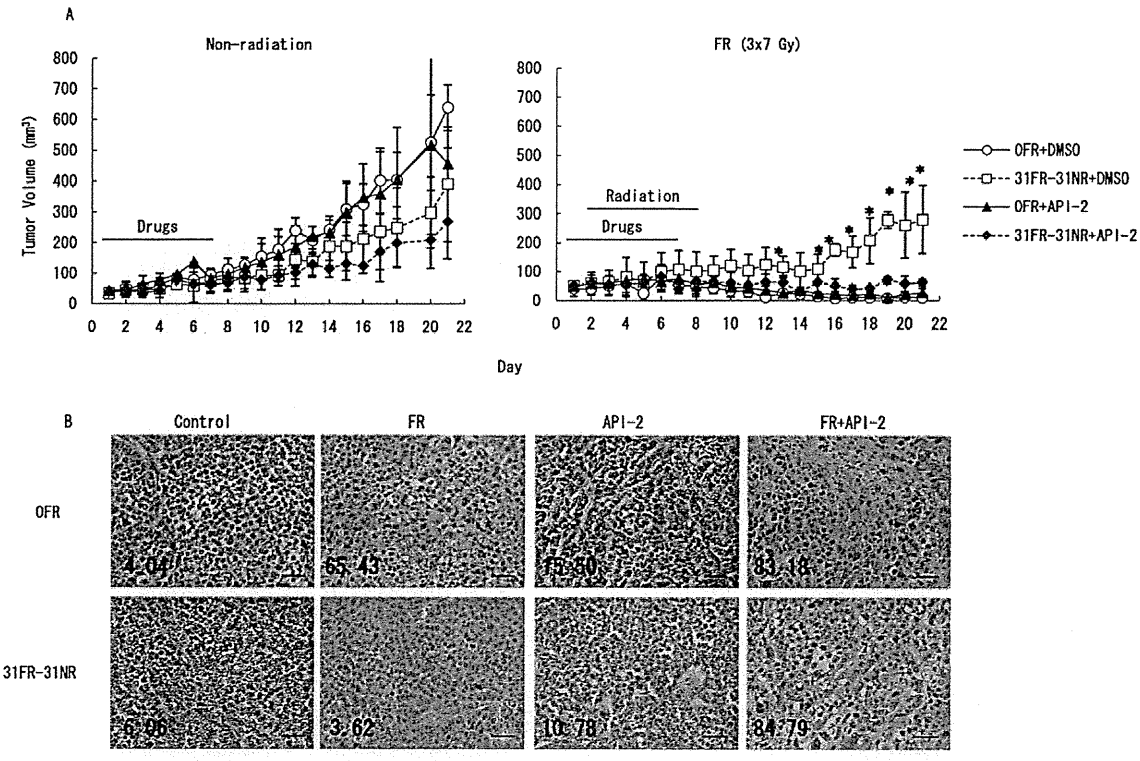

Fig. 5. Suppression of *in vivo* radioresistance of 31FR-31NR tumors by AKT inactivation. (A) *In vivo* tumor growth of 0 fractionated radiation (FR) and 31FR-31NR tumors. Mice were treated with DMSO (vehicle), 1 mg/kg/day API-2, FR (3 Gy × 7) with DMSO and FR with API-2. (B) Histological sections of tumors on day 21 were made and stained with hematoxylin and eosin. 0FR and 31FR-31NR tumors treated with DMSO alone, API-2 alone, FR with DMSO, and FR with API-2. Scale bar is 50 μm. Percentage of dead cells was shown in pictures. We counted more than 100 cells at each image.

observed in tumors with FR and the difference was prominent between DMSO and API-2 groups of 31FR-31NR tumors (Fig. 5B). Thus, inhibition of the AKT/GSK3β/cyclin D1 pathway could be promising for suppression of tumor radioresistance.

DISCUSSION

RT has been one of the most effective nonsurgical treatments for cancer; however, tumor radioresistance limits the effectiveness of RT and prevents tumors from complete eradication (1). We have recently revealed that tumor cells acquire radioresistance following long-term FR, and that acquired radioresistance is stably long-lasting for at least 1 month after cessation of FR (2). In the present study, we demonstrated that 31FR-31NR HeLa cells with acquired radioresistance resisted to 2 Gy of FR *in vitro* and 3 Gy of FR *in vivo*. Interestingly, radioresistance to FR was detectable in 31FR-31NR HepG2 cells at 1.5 Gy/fraction/day, but not at 2 Gy/fraction/day. These results indicate that the extent of radioresistance to FR is correlated with intrinsic radiosensitivity of parental cells even though radioresistance is acquired by FR.

The PI3K/AKT pathway is activated by upstream growth signals from a variety of growth factor receptor tyrosine kinases. This pathway is also upregulated after irradiation (11, 17) and is tightly correlated with tumor radioresistance in many cancers (3–7). AKT is known to block apoptotic pathways by regulating various target molecules including proapoptotic and antiapoptotic proteins (18, 19). Active AKT, a common mediator of cell survival signals induced by radiation through multiple intracellular signaling pathways, modulates apoptosis and increases the apoptotic threshold (20, 21). Thus, a cell fate may be determined by a balance between cell survival and apoptosis after irradiation in tumor cells.

Although AKT is involved in regulation of cell survival and proliferation, downstream targets of the AKT signaling pathway responsible for tumor radioresistance have not yet been clarified. In the present study, we showed that the blockade of the activated AKT/GSK3β/cyclin D1 pathway by API-2 rendered 31FR-31NR cells susceptible to FR with increased apoptosis. Also incidence of apoptosis significantly increased after irradiation by treatment with Cdk4-I in 31FR-31NR cells. Cdk4-I, but not API-2, radiosensitized the cells with cyclin D1-T286A. Thus, API-2 was ineffective in reducing radioresistance of tumor cells overexpressing cyclin D1-T286A. These results demonstrated that cyclin D1/Cdk4 is the most important AKT target for tumor radioresistance against fractionated RT.

Because of the expansion of understanding of the molecular mechanisms underlying radioresistance, the combination of molecular-targeted agents and irradiation is now being applied for cancer treatment (22, 23). We presented here that treatment with API-2 alone did not have effects on induction

of cell death in HeLa cells. In addition, no detectable side effects on body weight or activity were observed in mice treated by the combination of FR and API-2 in the present study. However, further investigation is required to confirm the feasibility of API-2 in RT. This study is the first to demonstrate that radioresistance and CDDP-resistance in cells acquired by long-term FR can be suppressed by targeting the AKT/GSK3β/cyclin D1/Cdk4 pathway. The present study suggests the importance of the cyclin D1 for manipulation of radiosensitivity and chemosensitivity in tumor cells, and the AKT/GSK3β/cyclin D1/Cdk4 pathway may serve as a new target to enhance efficacy of RT.

REFERENCES

1. Kim JJ, Tannock IF. Repopulation of cancer cells during therapy: An important cause of treatment failure. *Nat Rev Cancer* 2005;5:516–525.
2. Shimura T, Kakuda S, Ochiai Y, *et al.* Acquired radioresistance of human tumor cells by DNA-PK/AKT/GSK3 beta-mediated cyclin D1 overexpression. *Oncogene* 2010;29:4826–4837.
3. Kim TJ, Lee JW, Song SY, *et al.* Increased expression of pAKT is associated with radiation resistance in cervical cancer. *Br J Cancer* 2006;94:1678–1682.
4. Tanno S, Yanagawa N, Habiro A, *et al.* Serine/threonine kinase AKT is frequently activated in human bile duct cancer and is associated with increased radioresistance. *Cancer Res* 2004; 64:3486–3490.
5. Bussink J, van der Kogel AJ, Kaanders JHAM. Activation of the PI3-K/AKT pathway and implications for radioresistance mechanisms in head and neck cancer. *Lancet Oncol* 2008;9: 288–296.
6. Schuurbiers OCJ, Kaanders JHAM, van der Heijden HFM, *et al.* The PI3-K/AKT-pathway and radiation resistance mechanisms in non-small cell lung cancer. *J Thorac Oncol* 2009;4: 761–767.
7. Gupta AK, McKenna WG, Weber CN, *et al.* Local recurrence in head and neck cancer: Relationship to radiation resistance and signal transduction. *Clin Cancer Res* 2002;8:885–892.
8. Manning BD, Cantley LC. AKT/PKB signaling: Navigating downstream. *Cell* 2007;129:1261–1274.
9. Vivanco I, Sawyers CL. The phosphatidylinositol 3-kinase-AKT pathway in human cancer. *Nat Rev Cancer* 2002;2:489–501.
10. Bozulic L, Surucu B, Hynx D, *et al.* PKB alpha/Akt1 acts downstream of DNA-PK in the DNA double-strand break response and promotes survival. *Molecular Cell* 2008;30: 203–213.
11. Li HF, Kim JS, Waldman T. Radiation-induced Akt activation modulates radioresistance in human glioblastoma cells. *Radiat Oncol* 2009;4:43.
12. Alt JR, Cleveland JL, Hannink M, *et al.* Phosphorylation-dependent regulation of cyclin D1 nuclear export and cyclin D1-dependent cellular transformation. *Genes Development* 2000;14:3102–3114.
13. Bommi-Reddy A, Almeciga I, Sawyer J, *et al.* Kinase requirements in human cells: III. Altered kinase requirements in VHL-/- cancer cells detected in a pilot synthetic lethal screen. *Proc Natl Acad Sci U S A* 2008;105:16484–16489.
14. Yang L, Dan HC, Sun M, *et al.* Akt/protein kinase B signaling inhibitor-2, a selective small molecule inhibitor of Akt signaling with antitumor activity in cancer cells overexpressing Akt. *Cancer Res* 2004;64:4394–4399.
15. Shimura T, Toyoshima M, Adiga SK, *et al.* Suppression of replication fork progression in low-dose-specic p53-dependent S-phase DNA damage checkpoint. *Oncogene* 2006;25:5921–5932.
16. Biliran H, Wang Y, Banerjee X, *et al.* Overexpression of cyclin D1 promotes tumor cell growth and confers resistance to cisplatin-mediated apoptosis in an elastase-myc transgene-expressing pancreatic tumor cell line. *Clin Cancer Res* 2005; 11:6075–6086.
17. Zingg D, Riesterer O, Fabbro D, *et al.* Differential activation of the phosphatidylinositol 3'-kinase/Akt survival pathway by ionizing radiation in tumor and primary endothelial cells. *Cancer Res* 2004;64:5398–5406.
18. Nicholson KM, Anderson NG. The protein kinase B/Akt signalling pathway in human malignancy. *Cell Signal* 2002;14: 381–395.
19. Duronio V. The life of a cell: Apoptosis regulation by the PI3K/PKB pathway. *Biochem J* 2008;415:333–344.
20. Dent P, Yacoub A, Contessa J, *et al.* Stress and radiation-induced activation of multiple intracellular signaling pathways. *Radiat Res* 2003;159:283–300.
21. Schmidt-Ullrich RK, Contessa JN, Dent P, *et al.* Molecular mechanisms of radiation-induced accelerated repopulation. *Radiat Oncol Invest* 1999;7:321–330.
22. Belka C, Jendrossek V, Pruschy M, *et al.* Apoptosis-modulating agents in combination with radiotherapy-current status and outlook. *Int J Radiat Oncol Biol Phys* 2004;58:542–554.
23. Dutreix M, Cosset JM, Sun JS. Molecular therapy in support to radiotherapy. *Mutat Res Rev Mutat Res* 2010;704:182–189.

Citation: Cell Death and Disease (2011) 2, e177; doi:10.1038/cddis.2011.56

www.nature.com/cddis

Enhancement of autophagy is a potential modality for tumors refractory to radiotherapy

Y Kuwahara[1], T Oikawa[1], Y Ochiai[1], MH Roudkenar[2], M Fukumoto[1], T Shimura[1], Y Ohtake[3], Y Ohkubo[3], S Mori[4], Y Uchiyama[5] and M Fukumoto*[,1]

Radiotherapy is a well-established treatment for cancer. However, the existence of radioresistant cells is one of the major obstacles in radiotherapy. In order to understand the mechanism of cellular radioresistance and develop more effective radiotherapy, we have established clinically relevant radioresistant (CRR) cell lines, which continue to proliferate under daily exposure to 2 Gray (Gy) of X-rays for >30 days. X-ray irradiation significantly induced autophagic cells in parental cells, which was exiguous in CRR cells, suggesting that autophagic cell death is involved in cellular radiosensitivity. An autophagy inducer, rapamycin sensitized CRR cells to the level of parental cells and suppressed cell growth. An autophagy inhibitor, 3-methyladenine induced radioresistance of parental cells. Furthermore, inhibition of autophagy by knockdown of *Beclin-1* made parental cells radioresistant to acute radiation. These suggest that the suppression of autophagic cell death but not apoptosis is mainly involved in cellular radioresistance. Therefore, the enhancement of autophagy may have a considerable impact on the treatment of radioresistant tumor.

Cell Death and Disease (2011) **2,** e177; doi:10.1038/cddis.2011.56; published online 30 June 2011
Subject Category: Cancer

Radiotherapy and radiochemotherapy are well-established treatment modalities for various cancers. Tumor cells have the capacity to cope with radiotherapy and chemotherapy through multiple pathways of growth arrest and cell death.[1] Various modes of cell death have been known, such as necrosis, apoptosis, accelerated senescence, mitotic catastrophe and autophagic cell death.[2–4] Among these, apoptosis has been the most extensively studied and has revealed to be the primary mode of cell death in leukemia and lymphoma cells.[5] However, the concept of cell death is continuously evolving and the role of apoptosis in radiation or anticancer drug treatment is being reappraised.[6] Although death after irradiation in leukemia and lymphoma is preceded by apoptotic changes, apoptosis has little or even no role in the killing of epithelial neoplastic cells by radiation.[7] Moreover, early response of cell death, apoptosis is not necessarily correlated with overall tumor sensitivity to anticancer treatment.[8,9]

Compared with other cell death patterns, autophagy induced by radiation or anticancer drugs is less studied.[4] Dual role of autophagy has been reported, cell death and survival. Therefore, autophagy is considered to be a double-edged sword in the process of tumor development.[10] Autophagy suppresses tumor formation by triggering a non-apoptotic cell death program. The *Beclin-1* gene, an ortholog of *Apg6*, which participates in the induction of autophagy in response to starvation is reported to be one of tumor-suppressor genes.[11] On the contrary, the activation of autophagy may permit cancer cells to survive within the nutrient-poor environment.[12] Anticancer drug-induced autophagy can lead either to cell death or alternatively to protection against cell death. An anticancer drug, tamoxifen induces autophagic cell death in human mammary carcinoma MCF-7 cells.[13] By contrast, in response to sulindac and tumor necrosis factor-α, autophagy is induced as a cell survival mechanism.[14–16] Autophagy may protect some cancer cells from ionizing radiation possibly by removing damaged macromolecules and organelles such as mitochondria, which could protect against apoptosis and allow continued survival of transformed cells.[17] Ionizing radiation does not induce apoptosis but induces autophagic changes in glioblastoma cell lines irrespective of their relative radiosensitivity.[18] It is suggested that a basal enhanced level of autophagy in cancer cells contributes to therapy resistance but prolonged activation of autophagy may lead to cell death by cellular self-degradation.[19]

In order to develop more effective tumor radiotherapy, we have recently established clinically relevant radioresistant (CRR) cell lines, HepG2-8960-R and HepG2-R from HepG2, and SAS-R from SAS, independently.[20,21] These cells continue to proliferate with daily exposure to 2 Gray (Gy) of X-rays for >30 days, which corresponds to the standard protocol of fractionated radiotherapy for cancer treatment. This study revealed that CRR cells were refractory to the induction of autophagy after irradiation and that facilitation of

[1]Department of Pathology, Institute of Development, Aging and Cancer, Tohoku University, Sendai, Japan; [2]Research Center, Iranian Blood Transfusion Organization, Tehran, Iran; [3]Department of Radiopharmacology, Tohoku Pharmaceutical University, Sendai, Japan; [4]Department of Maxillofacial Surgery, Graduate School of Dentistry, Tohoku University, Sendai, Japan and [5]Department of Cell Biology and Neuroscience, Juntendo University Graduate School of Medicine, Tokyo, Japan
*Corresponding author: M Fukumoto, Department of Pathology, Institute of Development, Aging and Cancer, Tohoku University, Sendai 980-8575, Japan.
Tel: +81 22 717 8507; Fax: +81 22 717 8512; E-mail: fukumoto@idac.tohoku.ac.jp
Keywords: radioresistant cells; radiotherapy; autophagy; rapamycin; 3-methyladenine
Abbreviations: CRR, clinically relevant radioresistant; RPM, rapamycin; HDS, high-density survival; 3-MA, 3-methyladenine; FR, fractionated radiation; Gy, Gray; RPMI, Roswell Park Memorial Institute; PBS, phosphate-buffered saline; RT, room temperature; AR, acute radiation
Received 14.12.10; revised 09.5.11; accepted 09.5.11; Edited by A Stephanou

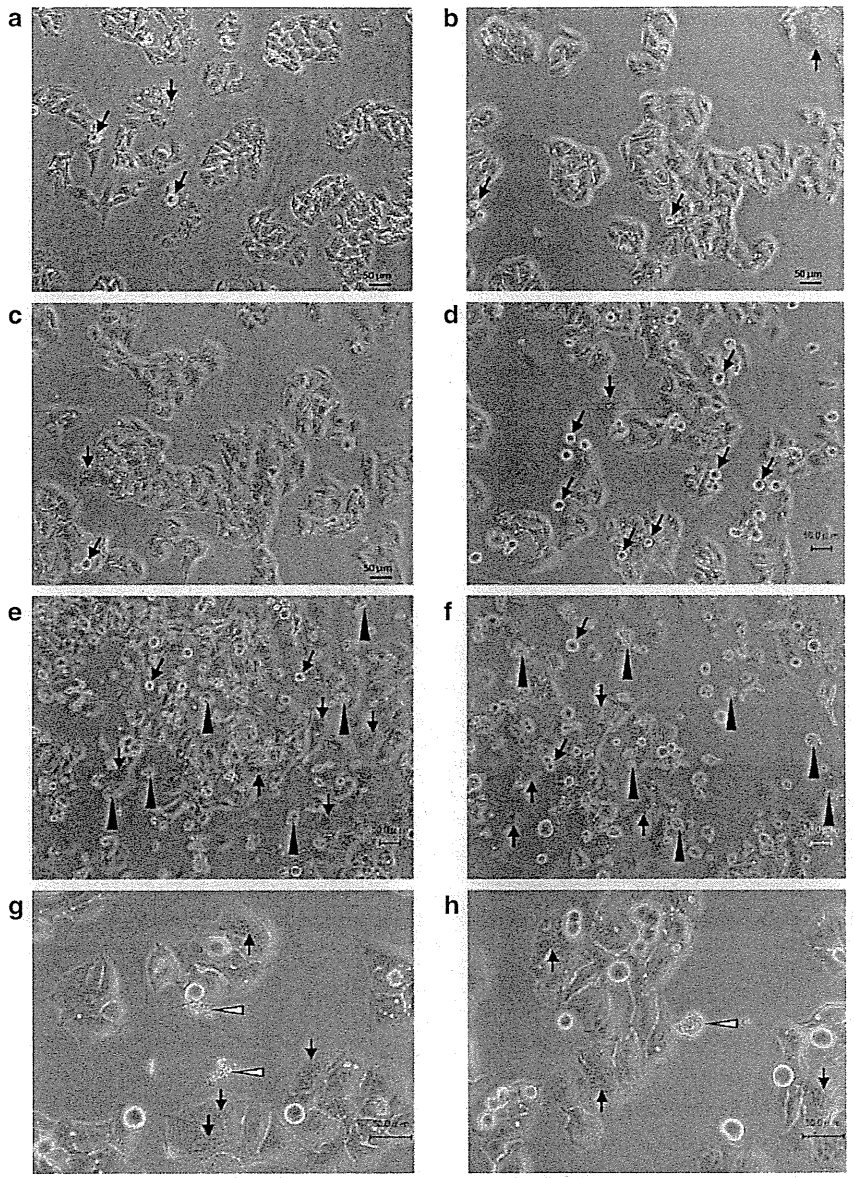

Figure 1 Microscopic appearance of parental HepG2 cells after exposure to a single dose of 10-Gy X-rays. (**a**) Mitotic figures but a few were observed in HepG2 cells without irradiation. (**b**) No remarkable changes but the increase in cell size were observed 1 day after exposure. (**c**) The increase in cell size was obvious 2 days after exposure. (**d**) Mitotic figures were apparent 3 days after exposure (black arrows). (**e**) At day 5 after exposure, a frequent number of dying cells were seen (black arrow heads). Multinucleated cells showing mitotic catastrophe were also increased (white arrows). (**f**) At day 7 after exposure. (**g**) Dead cells with apoptotic bodies (arrow heads; 5 days after exposure to X-rays). (**h**) Dead cell without apoptotic bodies (arrow head; 5 days after exposure to X-rays)

autophagy by rapamycin (RPM) abrogated the CRR phenotype. We also found that repression of autophagy induced radioresistance in non-CRR parental cells.

Results

Microscopic analysis of radiation-induced cell death after acute exposure to 10 Gy of X-rays. We pursued morphological changes characteristic to radiation-induced cell death. Within 2 days after 10 Gy of acute radiation (AR), prominent changes in morphology were not observed in HepG2 cells other than a slight increase in the cell size (Figures 1a–c). At day 3 after AR, the number of round cells, that is, mitotic cells increased (Figure 1d). Thereafter dead cells became obvious and multinucleated cells, characteristic to mitotic catastrophe, were also observed (Figures 1e and f). Dying cells were classified into two types: apoptotic cells with apoptotic bodies (Figure 1g) and non-apoptotic cells without apoptotic bodies (Figure 1h). The frequency of non-apoptotic cells was significantly higher than that of apoptotic cells.

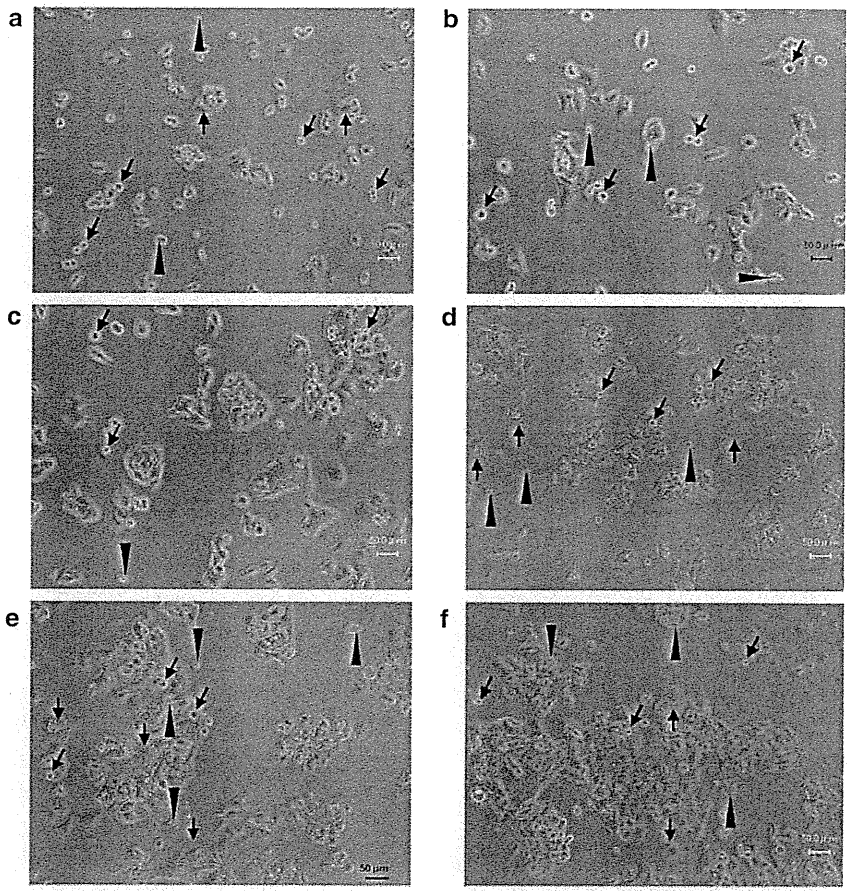

Figure 2 Microscopic appearance of radioresistant HepG2-8960-R cells after acute exposure to 10 Gy of X-rays. (**a**) HepG2-8960-R cells 2 days after exposure to 2 Gy of X-rays (maintenance irradiation). Mitotic cells (black arrows), dead cells (black arrow heads) and multinucleated cells showing mitotic catastrophe (white arrows) were observed. (**b**) No remarkable changes were observed 1 day after exposure to 10 Gy of X-rays. (**c**) Unlike HepG2 cells the increase in cell size was not obvious 2 days after exposure to 10 Gy of X-rays. (**d**) Mitotic figures were not apparent compared with HepG2 cells 3 days after exposure to 10 Gy of X-rays. (**e**) At day 5 after exposure to 10 Gy of X-rays, the frequency of dead cells was lower compared with HepG2. (**f**) At day 7 after exposure to 10 Gy of X-rays, the number of cells in mitotic catastrophe was not increased

Basal levels of dead cells were higher in radioresistant HepG2-8960-R than HepG2 (Figure 2a), presumably due to maintenance irradiation at 2 Gy per day. During this experimental period, distinguishable induction of cell death was not observed (Figures 2a–f). At day 3 after AR, inconsiderable increase in non-apoptotic cell death was observed in HepG2-8960-R (Figure 2d). After that no increase in either dead cells or mitotic catastrophe was observed (Figures 2e and f). These suggested that apoptosis is not a major type of cell death induced by ionizing radiation.

To examine to what extent X-ray exposure induces apoptotic changes, apoptotic cell death was evaluated by different methods. Basal level of annexin V-positive apoptotic cells observed under a microscope was significantly higher in HepG2-8960-R than in HepG2 (Figure 3a). AR of 10 Gy increased the frequency of annexin V-positive cells both in HepG2 and HepG2-8960-R. The increase was faster and higher in HepG2-8960-R than that in HepG2. The maximum level was about 20% in HepG2-8960-R and 10% in HepG2. The frequency of annexin V-positive cells was constant in both cell lines after reaching the maximal level. On the other hand, fractionated radiation (FR) of 2 Gy per day did not induce significant frequency of annexin V-positive cells both in HepG2 and HepG2-8960-R (Figure 3b). We next examined DNA ladder formation, a hallmark of apoptosis. Although 5 days after AR, many dead cells were observed in the cell culture (Figure 1e), DNA ladder formation was not observed in both HepG2 and HepG2-8960-R at any time examined (Supplementary Figure S1A). Radiation-induced DNA ladder formation was not detectable in SAS and SAS-R (Supplementary Figure S1B). We further examined the expression of cleaved caspase 3 after irradiation. After AR, significant increase in cleaved caspase 3 was not detectable by western blotting from 0 to 7 days after AR in all cell lines examined (data not shown). Radiosensitivity under the inhibition of apoptosis by Z-VAD-FMK was evaluated. The inhibition of apoptosis sensitized both HepG2 and HepG2-8960-R to X-rays slightly at lower doses and significantly at 10 Gy (Supplementary Figures S2A and B). However, the inhibition of apoptosis did not affect surviving fractions of SAS and

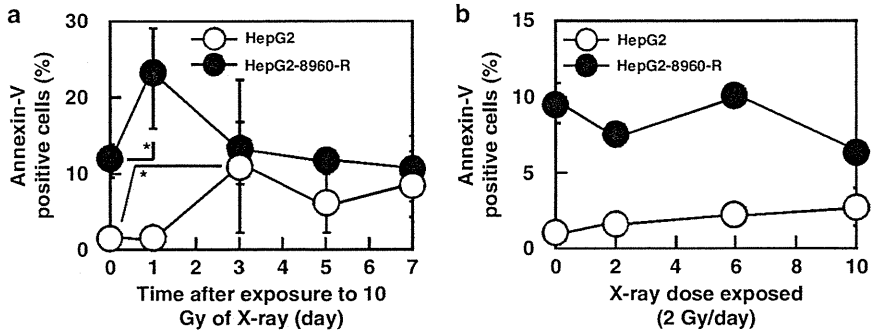

Figure 3 Frequencies of annexin V-positive cells induced by 10 Gy of a single dose of X-rays or fractionated X-rays. Basal levels of annexin V-positive cells in radioresistant HepG2-8960-R were higher than those in parental HepG2. (**a**) Annexin V-positive cells in HepG2 and HepG2-8960-R increased after acute exposure, however, induction level of annexin V-positive cells in HepG2 was higher than that in HepG2-8960-R. (**b**) Statistically significant induction of apoptosis was not observed both in HepG2 and HepG2-8960-R after exposure to fractionated 2 Gy of X-rays. Mean ± S.D. of three independent experiments. $^*P<0.05$ compared with control

SAS-R (Supplementary Figures S2C and D). These results indicated that contribution of apoptosis to cellular radiosensitivity is lower than previously considered.

Autophagy induced by X-ray exposure. We analyzed immunocytochemically positive cells for LC-3, a marker of autophagosomes. AR induced cells whose cytoplasm was filled with autophagosomes both in HepG2 and HepG2-8960-R (Figure 4). We defined these characteristic cells as 'hyperinduced autophagic cells' (Figures 4b and c). The frequency of hyperinduced autophagic cells in HepG2-8960-R (24.0 ± 5.2%) was significantly higher than that in HepG2 (1.5 ± 0.7%). Within 24 h after AR of 10 Gy, hyperinduced autophagic cells did not increase in both HepG2 and HepG2-8960-R (Supplementary Figure S3). Electron microscopic observation also confirmed that autophagic cell death was induced both in HepG2 and HepG2-8960-R by AR (Figures 4e–h). The frequency of hyperinduced autophagic cells in HepG2 gradually increased from day 3 and reached 78.2 ± 6.1% at day 7 after AR (Figure 5a). On the contrary, marked induction of hyperinduced autophagic cells was not observed in HepG2-8960-R and the frequency was 40.9 ± 8.6% at day 7. Exposure to 5 × 2 Gy of FR remarkably induced hyperinduced autophagic cells in HepG2 (45.9 ± 6.9%) but not in HepG2-8960-R (24.2 ± 1.8%; Figure 5b). We next examined the conversion of LC3-I to LC3-II, which is an indicator of autophagic activity and the amount of LC3-II correlates well with the number of autophagosomes.[22] At day 5 after AR, LC3-II level increased in both HepG2 and HepG2-8960-R, and the induction level was higher in HepG2 than in HepG2-8960-R (Figure 5c). We further examined the expression level of p62, which accumulates when autophagy is inhibited and decreases when autophagy is induced.[23] Without irradiation the expression level of p62 in HepG2 was higher than that in HepG2-8960-R (Figure 5d). The expression of p62 in HepG2 remained reduced from day 3 to 7 after AR and that in HepG2-8960-R reduced at day 3 but returned to the basal level by day 7.

Radiosensitization of CRR cells via induction of autophagy. Radiosensitivity after facilitation of autophagy by RPM was evaluated. Chronic exposure to radiation reduces plating efficiency on which reproducibility of clonogenic assay depends. Therefore, in this study the modified high-density survival (HDS) assay instead of clonogenic assay was used to determine cellular radiosensitivity. HepG2-8960-R and all other CRR cell lines examined were significantly radioresistant compared with their corresponding parental cell lines (Figure 6a, Supplementary Figure S4). Radiosensitivity of HepG2-8960-R with RPM treatment became almost the same as that of HepG2 (Figure 6b). RPM also sensitized both HepG2-R and SAS-R (Supplementary Figures S4B and D) and its radiosensitizing effect tended to be higher at higher doses. Radiosensitivity of HepG2 with or without RPM was not significantly different (Supplementary Figure S5A). The inhibition of autophagy by 3-methyladenine (3-MA) did not radiosensitize HepG2-8960-R (Supplementary Figure S5D), but made HepG2 radioresistant to the level of HepG2-8960-R and even more resistant than HepG2-R (Figure 6C and Supplementary Figure S6B). Radioresistance was also induced in SAS by 3-MA (Supplementary Figure S6D). However, these effects were not observed in both HepG2-R and SAS-R (Supplementary Figures S6B and D).

Autophagy induced by FR. RPM at the concentration of 10 ng/ml for 5 days was not toxic to HepG2 (Figure 7a), but significantly suppressed cell growth of HepG2-8960-R at day 5 (Figure 7b). FR alone suppressed cell growth of HepG2 (Supplementary Figure S7A), but additional radiosensitizing effect of RPM was not detected (Figure 7c). On the other hand, cell growth of HepG2-8960-R was drastically suppressed by the administration of FR and RPM (Figure 7d) and this effect was reinforced by FR (Supplementary Figure S7D).

Cell growth of HepG2 was suppressed by 3-MA (Figure 7e). The effect of 3-MA on the cell growth was not obvious in HepG2-8960-R (Figure 7f). Radiosensitizing effect of 3-MA on FR was not observed both in HepG2 (Figure 7g, Supplementary Figure S7E) and in HepG2-8960-R (Figure 7h, Supplementary Figure S7F).

Radiosensitizing effect of RPM was also confirmed in HepG2-R and SAS-R cells but not in SAS cells, indicating that the CRR phenotype is reversed by RPM (Supplementary

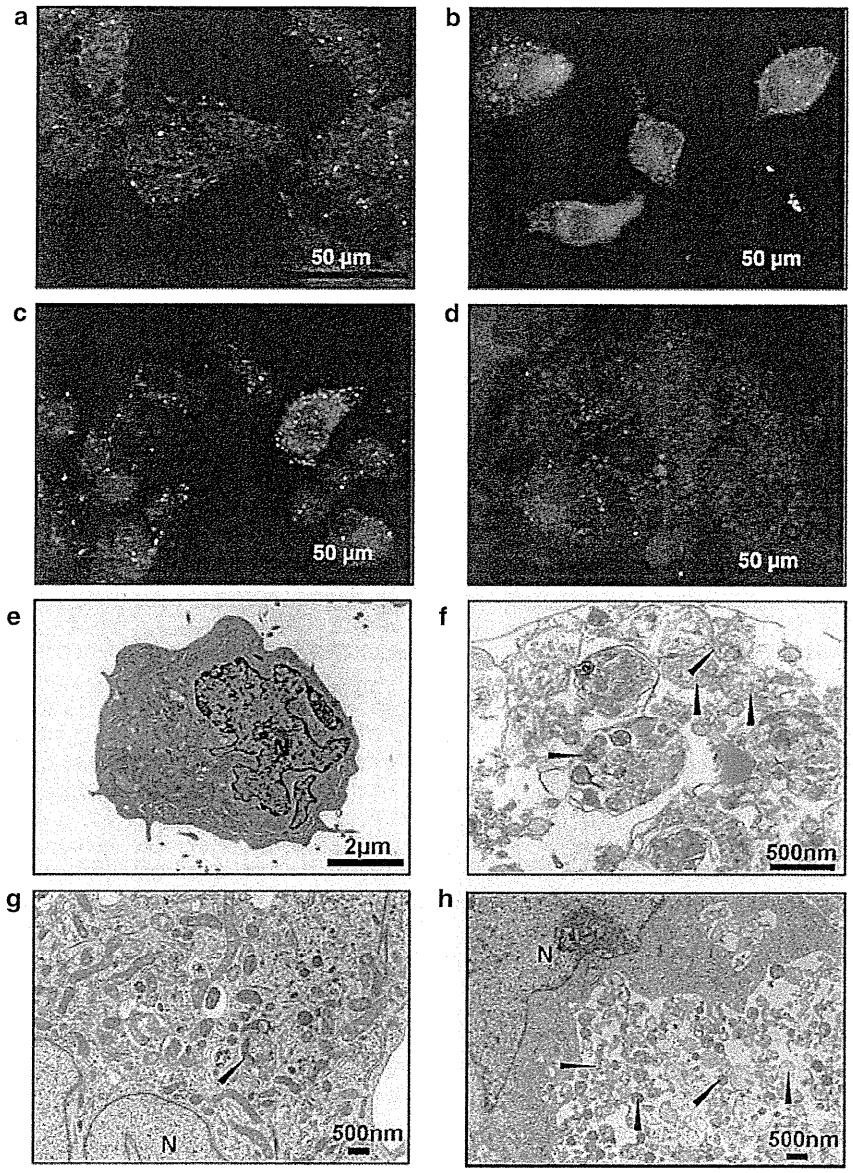

Figure 4 (**a**–**d**) Representative figures of hyperinduced autophagic cells by a single dose of 10-Gy X-rays in parental HepG2 and radioresistant HepG2-8960-R cells. Autophagosomes were immunocytochemically visualized by anti-LC-3 antibody and cells filled with autophagosomes were counted as hyperinduced autophagic cells (arrows). (**e**–**h**) Electron microscopic analysis of HepG2 and HepG2-8960-R. (**a**) Hyperinduced autophagic cells were seldom observed in HepG2 cells without irradiation. (**b**) At day 7 after exposure to 10 Gy of X-rays, the level of hyperinduced autophagic HepG2 cells was 78.2 ± 6.1%. (**c**) HepG2-8960-R cells 2 days after the last maintenance irradiation (2 Gy per day). (**d**) At day 7 after exposure to 10 Gy of X-rays, significant induction of hyperinduced autophagic cells was not observed in HepG2-8960-R. (**e**) HepG2 cells without X-rays. (**f**) At day 5 after exposure to 10 Gy of X-rays, HepG2 cells were filled with autophagosomes (arrow head). (**g**) HepG2-8960-R cell 2 days after the last maintenance irradiation (2 Gy per day). (**h**) HepG2-8960-R cell filled with autophagosomes at day 5 after exposure to 10 Gy of X-rays

Figures S8B, D and F). On the other hand, administration of 3-MA conferred radioresistance on SAS against FR (Supplementary Figure S8D).

We next examined whether administration of RPM or 3-MA induces apoptosis, mitotic catastrophe or hyperinduced autophagic cells. At day 5 after irradiation, the frequency of annexin V-positive cells was not significantly different between with or without RPM or 3-MA (Supplementary Figure S9A). The induction frequency of mitotic catastrophe was not different between HepG2 and HepG2-8960-R irrespective of RPM or 3-MA treatments (Supplementary Figure S9B). Although RPM increased the frequency of hyperinduced autophagic cells in HepG2-8960-R 7 days after AR, unexpectedly did not in HepG2. Administration of 3-MA suppressed X-ray-induced hyperinduced autophagic cells in HepG2 (Supplementary Figure 9C).

Beclin-1 knockdown and radiosensitivity. We further examined whether inhibition of autophagy by knockdown of *Beclin-1* induces radioresistance or not. We used psiRNA-